sustainability

MDPI

Article

From Prediction to Causal Inference: Multi-Model Double Machine Learning for Life-Cycle Carbon Optimization of RAP Mixtures

Minda Ren [1], Zian Pei [2], Xin Luo [3], Jian Gao [3] and Lan Wang [1,*]

[1] Inner Mongolia Key Laboratory of Green Construction and Intelligent Operation and Maintenance of Civil Engineering, School of Civil Engineering, Inner Mongolia University of Technology, Hohhot 010051, China; m_ren@imut.edu.cn
[2] School of Civil Engineering, Inner Mongolia University of Technology, Hohhot 010051, China; peizian0816@163.com
[3] Inner Mongolia Transportation Group Mengtong Maintenance Co., Ltd., Hohhot 010051, China; luoxinkj@126.com (X.L.); nmgmtyh@126.com (J.G.)
* Correspondence: wanglan661018@163.com

Abstract

Efficient recycling of reclaimed asphalt pavement (RAP) is essential to the low-carbon transformation of transportation infrastructure. Traditional carbon accounting methods based on four factors—RAP content, aging level, rejuvenator dosage, and mixing temperature—struggle to capture emission patterns under multi-parameter coupling or isolate confounders to identify true causal effects. The study considers a single-lane asphalt pavement functional unit (1 km length, 3.75 m width, and 0.18 m thickness), and to address this problem, this paper integrates life cycle assessment (LCA), a thermodynamic mechanism model, multi-model machine learning, and double/debiased machine learning (DML) to construct a carbon emission prediction and causal analysis framework. First, reclaimed asphalt pavement is used as the LCA model to generate 10,206 carbon emissions and cost datasets covering the four factors, with embedded nonlinear thermodynamic calculations. Then, 3000 semi-synthetic plant-day observations are constructed by introducing observable engineering conditions, batch variation, and Gaussian white noise. Finally, four prediction models—BP neural network, random forest, XGBoost, and SVR-RBF—were compared using grouped five-fold cross-validation. The BP model achieved the highest predictive accuracy ($R^2 = 0.9638$) and was selected as the auxiliary learner for cross-fitted DML. The estimated model-based intervention effects for a 10-percentage-point increase in RAP content, a 0.1 increase in aging coefficient, a 1-percentage-point increase in rejuvenator dosage, and a 10 °C increase in mixing temperature were 12.492, 7.077, 13.189, and 8.632 t CO_2-eq, respectively. These results show that material circularity and carbon reduction do not automatically guarantee economic sustainability. The framework links resource circularity, causal process understanding, and low-carbon process optimization to support sustainability-oriented RAP decisions. This study offers a reference for low-carbon design and process optimization of asphalt pavement recycling.

Keywords: sustainability; reclaimed asphalt pavement (RAP); life cycle assessment (LCA); causal inference; double machine learning (DML); random forest; XGBoost; support vector regression

Check for updates

Academic Editor: Rui Micaelo

Received: 28 July 2026
Revised: 25 September 2026
Accepted: 14 October 2026
Published: 23 October 2026

Copyright: © 2026 by the authors. Licensee MDPI, Basel, Switzerland. This article is an open access article distributed under the terms and conditions of the Creative Commons Attribution (CC BY) license.

1. Introduction

Reclaimed asphalt pavement (RAP) technology, by recycling old asphalt pavement materials, can effectively reduce the consumption of new materials, lower the pressure of waste disposal, and achieve certain carbon emission reduction benefits [1–5]. Research has shown that incorporating RAP can reduce carbon emissions during asphalt mixture production to some extent, but the relationship between RAP content and its emission reduction benefit is not strictly proportional. As RAP content increases, the introduction of aged asphalt, the addition of rejuvenators, and the increased energy consumption for pre-treatment can lead to reduced workability and impaired durability of the mixture, resulting in a rebound in carbon emissions [6]. Furthermore, among the key factors influencing the carbon emissions of recycled asphalt mixtures, RAP content is not the sole determinant. Studies indicate that RAP content, degree of aging, rejuvenator dosage, and mixing temperature are the four major factors affecting the carbon emission benefits of recycled asphalt mixtures. At present, the complex causal mechanisms through which factors such as RAP content, aging degree, rejuvenator dosage, and mixing temperature influence carbon emissions remain unclear. Traditional carbon accounting methods based on fixed coefficients struggle to accurately capture the patterns of emission variation under multi-parameter interactions, nor can they achieve dynamic optimization of process parameters.

Previous research on the sources of carbon emissions from asphalt pavements has mainly focused on the life cycle assessment (LCA) framework, with targeted analyses of the impact of individual factors on emissions. Early studies compared carbon emission differences at varying RAP contents and found that emission reduction is significant when RAP content is within 30%, but the benefit diminishes beyond 50% due to increased energy consumption [7]. Further research introduced energy consumption monitoring and thermodynamic models to quantify the carbon contributions of RAP preheating, screening, and other pre-treatment processes, indicating a nonlinear increase in emissions at high RAP contents [8]. In terms of analyzing parameter influence mechanisms, existing studies have explored the statistical relationships involving RAP content in recycled asphalt mixtures through correlation analysis, regression models, and sensitivity analysis. Some studies developed an improved regression fatigue prediction model for recycled asphalt mixtures based on strain level, asphalt content, air void ratio, and RAP content [9]. Correlation analysis by other researchers showed that RAP addition weakens the moisture sensitivity, crack resistance, and fatigue performance of recycled mixtures but enhances their permanent deformation resistance [10]. Another study used sensitivity analysis and other models to evaluate the probability that HMA life-cycle carbon emissions exceed those of CMA pavement systems [11]. Furthermore, research on two pre-treatment methods—fine disaggregation and conventional separation—demonstrated that RAP incorporation adversely affects the dispersion uniformity of aggregates in recycled asphalt mixtures [12]. In recent years, machine learning methods have shown strong potential in areas such as material performance prediction and process optimization. For instance, models like random forest and neural networks have been used to build carbon emission prediction models and identify key stages and influencing factors. One researcher found that XGBoost provides the most accurate carbon emission predictions compared to other machine learning models [13]. Other studies combined signal decomposition algorithms with nonlinear autoregressive neural networks and deep extreme learning machines to construct hybrid models for carbon emission prediction [14]. Several researchers compared multiple different models to identify the optimal one for carbon emission prediction [15–18]. Another study, targeting carbon emissions as the objective feature, developed various regression models and evaluated them based on root mean square error, coefficient of determination, and mean absolute percentage error, finding that a stacking ensemble model exhibited superior predictive

performance and further applied it to sensitivity analysis of carbon emission influencing factors [19]. However, as research progresses, certain gaps remain evident. Current studies predominantly focus on static carbon emission accounting, lacking dynamic analysis of the contribution of each life-cycle stage to emissions. Moreover, there is insufficient research on the synergistic optimization of RAP content and other process parameters, and a multi-parameter coupled prediction and optimization framework for carbon emissions has yet to be established [20].

Recent studies have increasingly distinguished predictive association from intervention questions. Accurate regression or artificial-intelligence prediction does not itself establish cause-and-effect relationships, and causal-discovery methods have begun to be applied in structural and construction engineering [21,22]. In asphalt materials, explainable machine learning, causal inference, and LCA have also been combined to investigate the sustainable design of fiber-reinforced asphalt concrete [23]. These developments are directly relevant to the present study because the 10,206 samples are generated by a programmed LCA/thermodynamic data-generating process rather than by a randomized field experiment. Accordingly, the causal statements in this paper are restricted to model-based intervention effects under explicit assumptions, observed engineering context, overlap, and nuisance-model adequacy, rather than being presented as experimentally verified real-world causal effects.

In summary, existing research has established LCA-based carbon emission accounting and machine learning prediction methods for recycled asphalt mixtures and has preliminarily revealed the nonlinear influence of individual process parameters. However, the understanding of carbon emission variations under multi-parameter coupling and engineering variability remains limited, and high prediction accuracy alone cannot determine the intervention effect of changing a single parameter after controlling for confounding conditions. This study therefore proposes a machine learning-assisted causal analysis framework integrating LCA, thermodynamic mechanism modeling, multi-model comparison, and DML. Specifically, 10,206 model-calculated LCA data points are first generated from RAP content, aging degree, rejuvenator dosage, and mixing temperature, after which observable plant operating conditions and Gaussian white noise are introduced to construct an engineering-perturbed dataset. Four models, including the BP neural network, random forest, XGBoost, and SVR-RBF, are then compared using grouped 5-fold cross-validation, and the model with the highest R^2 is selected before causal estimation to assist cross-fitted DML. Subsequently, the model-based intervention effects of the four process parameters and their robustness to white noise are analyzed. Finally, published asphalt-plant energy consumption data and representative engineering carbon-emission data are used as external engineering benchmarks. The proposed framework provides a systematic method for carbon emission prediction, parameter-effect identification, and low-carbon process optimization of RAP recycled asphalt mixtures, and therefore provides sustainability-oriented decision support for RAPs, while the causal interpretation remains conditional on the specified data-generating process and requires further field validation.

2. Methods

2.1. System Boundary and Functional Unit

Determining the system boundary is a crucial step in LCA. This study is a model-based case for a generic RAP recycled asphalt pavement layer rather than a laboratory-constructed named mixture. The modeled layer is evaluated from raw material acquisition to end-of-life/recycling through six physical stages: raw material acquisition, transportation, production, construction, use and maintenance, and end-of-life/recycling (Figure 1). The carbon-accounting standard DB15/T 3727-2024 [24] is used as one factor/source reference;

however, its ultra-thin warm-mix wearing-course scope should not be interpreted as defining the 0.18 m model geometry used here.

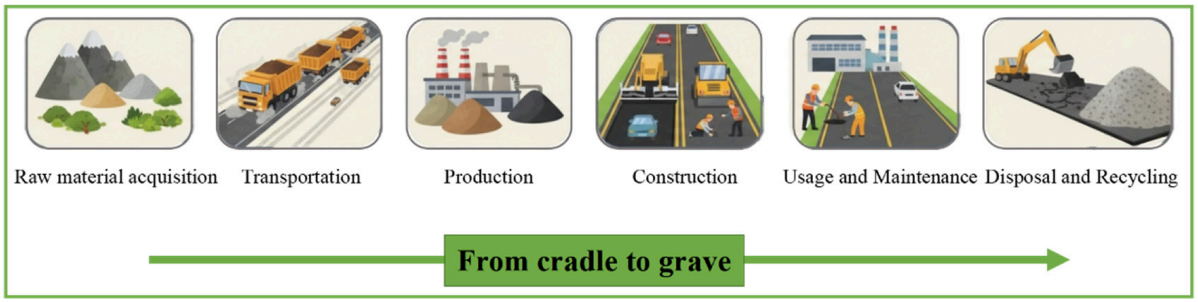


Figure 1. Asphalt pavement life cycle.

(1) Raw material acquisition stage, including the production energy consumption and process emissions of new asphalt(Panjin Northern Asphalt, Panjin, China), new aggregates (Jinglianxin Road-Use Materials Co., Ltd, Beijing, China), RAP crushing and screening, and rejuvenator (Kangdefumei Greenway Co., Ltd, Dezhou, China).

(2) Transportation stage, divided into raw material transportation and mixture transportation, where various materials are transported from their source or processing plants to the mixing plant.

(3) Production stage, including the energy consumption of processes such as aggregate drying, asphalt and RAP heating, and mixing.

(4) Construction stage, where the mixed asphalt mixture is transported to the construction site for paving and compaction. In this process, the mixture is evenly laid on the pavement using a screed-type paver (Xuzhou Construction Machinery Group Co., Ltd, Xuzhou, China); compaction is carried out by steel-wheeled rollers and rubber-tired rollers (Xuzhou Construction Machinery Group Co., Ltd, Xuzhou, China) to ensure the smoothness and stability of the road surface.

(5) Use and maintenance stage, considering preventive maintenance (micro-surfacing) and corrective maintenance (overlay) within the design life.

(6) End-of-life and recycling stage, including milling, landfilling, or secondary recycling after the pavement reaches the end of its service life.

The functional unit of the study is defined as a single-lane asphalt pavement layer with a length of 1 km, a width of 3.75 m, and a thickness of 0.18 m, with a mixture density of 2.4 t/m^3.

2.2. Data Inputs and Datasets

The study uses three categories of data for different purposes. First, design/LCA inputs define the functional unit, four process-factor grids, carbon emission factors, construction/transport energy use, cost parameters, and thermodynamic properties obtained from published specifications and literature sources. Second, the 10,206 model-generated factorial combinations define the deterministic mechanism/LCA response surface; they are not measured asphalt-mixture specimens and are not used as the primary engineering-generalization benchmark. In these combinations, RAP content denotes the mass fraction of RAP in the modeled mixture, aging degree is the RAP aging coefficient, rejuvenator dosage is the percentage of rejuvenator relative to total mixture mass, and mixing temperature is the production temperature. Third, a separate 3000-observation semi-synthetic plant-day layer combines the process settings with observable engineering context and stochastic disturbances for the main four-model grouped-CV comparison and DML robustness analysis. Published engineering data from asphalt mixing plants and representative pavement

projects are used to define plausible ranges for engineering-context variables and to check the order of magnitude of production-stage energy and carbon emissions. These external data are not merged with the 10,206 design points as labels and are not called external validation because system boundaries, plant fuels, mixture types, and functional units differ. Detailed information on data sources and basis is provided in Table 1.

Table 1. Data sources and basis.

Source/Author	Year	Data Type	Specific Parameters/Indicators
Ministry of Transport of the People's Republic of China [25]	2014	Functional unit and system boundary parameters	Pavement length (1 km), width (3.75 m), design life (15 years) Asphalt layer thickness (0.18 m)
Menghao Wang [26]	2023	Core process parameters and value ranges	1. RAP content: 0–100% (21 levels)
Pei Luo [27]	2025		2. Aging coefficient: 0.8–1.6 (9 levels)
Hao Li [28]	2022		3. Recycling agent content: 0–5% (6 levels)
Haibiao Fu [29]	2021		4. Mixing temperature: 140–180 °C (9 levels)
Inner Mongolia Autonomous Region Market Supervision Administration [24]	2024	Carbon emission factors	1. Raw material production: new asphalt (248), aggregate (201, average of three types: coarse aggregate, fine aggregate, mineral filler), recycling agent (950) (kg CO_2-eq/t)
			2. Energy: diesel (3.1), gasoline (2.929), heavy oil (3.06), coal (2.493), electricity (0.61) (kg CO_2-eq/unit)
			3. Waste treatment: landfill, recycling
		Energy consumption data of construction machinery	Fuel consumption per unit workload of asphalt pavers, mixing equipment, various transport vehicles(Xuzhou Construction Machinery Group Co., Ltd, Xuzhou, China), etc. (L/t or kg/t)
Ministry of Transport of the People's Republic of China [30] Shanghai Environment and Energy Exchange [31]	2018 2023	Cost and market price parameters	1. Material unit prices: new asphalt, aggregate, RAP, recycling agent, etc. (CNY/ton)
			2. Energy unit prices: diesel, electricity, coal, etc. (CNY/unit)
			3. Unit prices for transport, construction, maintenance, disposal (CNY/(ton·km) or CNY/ton)
			4. Carbon trading price (CNY/ton CO_2)
Editorial Committee of China Materials Engineering Canon [32] Yang, S.; Tao, W. [33]	2006	Thermodynamic and material property parameters	Aggregate specific heat capacity (0.92), asphalt specific heat capacity (1.67), moisture content Latent heat of vaporization of water (2260), thermal efficiency, etc. (kJ/(kg·°C))
Schönauer et al. [34]	2024	Primary asphalt-plant operational data	Daily production volume, mixture temperature, dryer starts and fuel use; high production associated with ~22% lower fuel/t; 186 to 162 °C associated with up to ~9% fuel saving
Wang et al. [35]	2024	Field-measured asphalt-plant production energy	AC-13: dust removal 3.623 kWh/t, drying 5.181 kg heavy oil/t, asphalt heating 1.561 kg natural gas/t, blending 7.302 kWh/t; used for production-stage plausibility
Schönauer et al. [36]	2026	Field trial for aggregate moisture	Aggregate moisture 1.46–9.83 mass%; +1 mass% moisture ≈ +6.86 kWh/t dryer energy; used to set moisture perturbation envelope
Kleizienė et al. [37]; Liu et al. [38]; NRCan [39]; Ma et al. [40]	2005–2025	Independent plant/ project engineering benchmarks	Per-tonne plant energy/carbon and project-scale GHG values used only for plausibility/context, not as labels or project-specific validation

2.2.1. Carbon Emission Factors for Raw Material Production

By referring to the technical specification for carbon emission accounting of ultra-thin wear layer using warm-mix recycled asphalt mixture, the relevant carbon emission factor data for the raw material stage of the life cycle can be obtained, as shown in Table 2.

Table 2. Carbon emission factors of major materials.

Stage	Item	Carbon Emission Factor	Unit
Raw material	New asphalt production	248	kg CO_2-eq/t
Raw material	Aggregate production	201	kg CO_2-eq/t
Raw material	Recycling agent production	950	kg CO_2-eq/t

2.2.2. Energy Consumption Values of Construction Machinery

By referring to the technical specification for carbon emission accounting of ultra-thin wear-resistant layer of warm-mix recycled asphalt mixture, the energy consumption values of machinery used in the transportation, production, and construction stages of the life cycle can be obtained, as shown in Table 3.

Table 3. Energy consumption of main construction machinery under a unit project.

Stage	Item	Energy	Energy Consumption Value	Unit
Production	Heater	Coal	0.135	kg/t
Production	Asphalt mixing equipment	Heavy oil	1.131	kg/t
Construction	Asphalt paver	Diesel	0.062	kg/t
Construction	Steel wheel roller	Diesel	0.024	kg/t
Construction	Pneumatic tire roller	Diesel	0.053	kg/t
Transport	Dump truck	Diesel	0.002	kg/t
Transport	Truck	Gasoline	0.003	kg/t
Transport	Liquid asphalt tanker	Diesel	0.085	kg/t
Transport	Mixture transport truck	Diesel	0.094	kg/t

2.2.3. Data Sources for Carbon Emission Factors

By referring to the technical specification for carbon emission accounting of ultra-thin wearing course using warm-mix recycled asphalt mixture, the carbon emission factors of energy sources used at each stage of the life cycle can be obtained, as shown in Table 4.

Table 4. Carbon emission factors of major energy sources.

Energy	Carbon Emission Factor (kg CO_2-eq/Unit)	Unit
Heavy oil	3.060	kg
Gasoline	2.929	kg
Diesel	3.100	kg
Coal	2.493	kg
Electricity	0.610	kW·h

2.3. Life-Cycle Carbon Emission Calculation Model

Carbon emissions are calculated for six physical life-cycle stages. E1–E6 denote raw material acquisition, transportation, production, construction, use/maintenance, and end-of-life/recycling, respectively. The total is $E_{total} = (E1 + E2 + E3 + E4 + E5 + E6 + E_{aux})/1000$, where E_{aux} contains only non-duplicated additional operations.

The original nonlinear functions are retained so that the study remains based on the submitted model, but their status is clarified. Asphalt-utilization efficiency, rejuvenator diminishing returns, RAP-related energy growth, construction difficulty, durability/maintenance frequency, and production-adjustment functions are scenario/calibration functions rather than universally validated constitutive laws. Their expressions, coefficients, sources or calibration status, and uncertainty ranges should be disclosed and stress-tested rather than presented as measured physical relationships.

2.3.1. Carbon Emission Quantification Model for the Raw Material Acquisition Stage

By calculating the new asphalt, aggregates, rejuvenator, and other raw materials according to Equation (1), the carbon emissions of this stage can be obtained.

$$C_{E1} = \sum m_i \alpha_i \quad (1)$$

where m_i is the consumption of the i-th raw material (t); α_i is the carbon emission factor corresponding to the production of the i-th raw material (kg CO_2-eq/t).

2.3.2. Carbon Emission Quantification Model for the Transportation Stage

This stage is divided into the transportation stage of raw materials and the transportation stage of the mixture. The emissions from different raw materials and the mixture, along with the corresponding machinery used, are calculated according to Equation (2).

$$C_{E2} = \sum \sum m_{ij} d_{ij} e_{ij} \alpha_k + \sum M_j d_j e_{jk} \alpha_k \quad (2)$$

where m_{ij} is the total amount of raw material i transported by machinery j (t); d_{ij} is the distance per ton of raw material i transported by machinery j (km); e_{ij} is the energy consumed by machinery j per ton-kilometer of raw material i (kg/t·km); α_k is the carbon emission factor corresponding to the k-th type of energy consumption (kg CO_2-eq/kg); M_j is the total amount of warm-mix recycled asphalt mixture transported by machinery j (t); d_j is the distance per ton of recycled asphalt mixture transported by machinery j (km); e_{jk} is the energy consumed by machinery j per ton-kilometer of recycled asphalt mixture (kg/t·km); and α_k is the carbon emission factor corresponding to the k-th type of energy consumption (kg CO_2-eq/kg).

2.3.3. Carbon Emission Quantification Model for the Production Stage

In this stage, the energy consumption required for heating raw materials such as asphalt, aggregates, and RAP, as well as for the mixing and preparation of the mixture, is calculated according to Equation (3).

$$C_{E3} = \sum M_m e_{jk} \alpha_k \quad (3)$$

where M_m is the total mass of the recycled asphalt mixture produced by mixing (t); e_{jk} is the energy consumed by machinery j per ton of recycled asphalt mixture during mixing (kg/t); and α_k is the carbon emission factor corresponding to the k-th type of energy consumption (kg CO_2-eq/kg).

2.3.4. Carbon Emission Quantification Model for the Construction Stage

This stage mainly accounts for the carbon emissions during the paving and rolling processes of the recycled asphalt mixture, which are calculated according to Equation (4).

$$C_{E4} = \sum M_P e_{jk1} \alpha_k + \sum M_n e_{jk2} \alpha_k \quad (4)$$

where M_p is the total mass of the recycled asphalt mixture being paved (t); e_{jk1} is the energy consumed by machinery j per ton of recycled asphalt mixture during paving (kg/t); α_k

is the carbon emission factor corresponding to the k-th type of energy consumption (kg CO_2-eq/kg); M_n is the total mass of the recycled asphalt mixture being rolled (t); and e_{jk2} is the energy consumed by machinery j per ton of recycled asphalt mixture during rolling (kg/t).

2.3.5. Thermodynamic Production Energy Consumption Model

To more accurately characterize the influence of temperature, a thermodynamic model based on energy conservation is constructed. This model calculates the total energy (sensible heat and latent heat) required to heat all components, including RAP, new aggregates, asphalt, and the contained moisture, from the ambient temperature to the target mixing temperature. It also accounts for heat losses and equipment efficiency, and finally normalizes the result into an energy consumption impact factor relative to the reference temperature (160 °C). The calculation is performed according to Equation (5).

$$Q_{total} = Q_{sensible} + Q_{latent} + Q_{loss} + Q_{special} \quad (5)$$

where Q_{total} is the total heat of the system (J); $Q_{sensible}$ is the sensible heat, i.e., the heat required to raise the temperature of the materials (J); Q_{latent} is the latent heat, i.e., the heat required for moisture evaporation (J); Q_{loss} is the heat loss, i.e., the heat dissipated to the environment (J); and $Q_{special}$ is the special energy consumption, i.e., energy consumed by RAP preheating, equipment efficiency losses, etc. (J).

2.3.6. Use and Maintenance Stage

For the current model, the number of preventive-maintenance and overlay events is determined by the design life and an RAP-dependent durability factor. The stage emission is $E5 = (N_m + N_o) \cdot M \cdot r_m \cdot EF_m$, where N_m and N_o are the numbers of maintenance and overlay interventions, M is the functional-unit mixture mass, r_m is the maintenance material ratio, and EF_m is the carbon factor used for the maintenance material. The maintenance rule and durability-factor intervals are scenario assumptions and should be included in uncertainty analysis.

2.3.7. End-of-Life and Recycling Stage

End-of-life emissions include transport/handling, secondary recycling, and landfill: $E6 = E_{EoL,transport} + M_{EoL} \cdot \eta_r \cdot EF_{recycle} + M_{EoL} \cdot (1 - \eta_r) \cdot EF_{landfill}$. Here M_{EoL} is end-of-life mass, η_r is assumed recycling efficiency, and $EF_{recycle}/EF_{landfill}$ are treatment factors. A negative recycling credit is an allocation assumption.

2.3.8. Parameterized Process Functions and Uncertainty Status

The predefined nonlinear functions are made explicit to improve reproducibility. Let r denote RAP mass fraction and q denote rejuvenator mass fraction. The asphalt-utilization coefficient is 0.75 for $r \leq 0.30$, 0.65 for $0.30 < r \leq 0.60$, and $0.55–0.10(r - 0.60)$ for $r > 0.60$. The rejuvenator-effect factor is $\max[0.40, 1 - 15q]$ for $q \leq 0.02$, $\max[0.40, 0.70 - 8(q - 0.02)]$ for $0.02 < q \leq 0.04$, and $\max[0.40, 0.54 - 4(q - 0.04)]$ for $q > 0.04$. The RAP production-energy factor is $1 + 0.8r$ for $r \leq 0.40$, $1.32 + 1.2(r - 0.40)$ for $0.40 < r \leq 0.70$, and $1.68 + 2.0(r - 0.70)$ for $r > 0.70$. Construction difficulty is represented by $1 + 0.3r^2$. The durability factor is 1.0, 0.9, and 0.8 for low-, medium-, and high-RAP ranges, respectively. Feeding sequence, mixing time, and temperature-control factors are also defined piecewise in the calculation code. Because these empirical coefficients are not calibrated against project-specific measurements, they are treated as scenario assumptions; their implications are therefore examined through engineering-context perturbation and white-noise robustness analyses rather than being presented as universally calibrated constitutive laws.

2.4. Extended Dataset Generation, Four-Model Comparison, and Auxiliary-Model Selection

By combining 21 RAP contents, 9 aging degrees, 6 rejuvenator dosages, and 9 mixing temperatures, an extended dataset of 10,206 deterministic LCA-calculated cases. These cases represent designed combinations of RAP recycled asphalt mixture process parameters and define the mechanism response surface. The dataset is used to analyze model-based emission variation and parameter interactions, while predictive benchmarking is conducted using the engineering-perturbation layer described below. The main prediction benchmark is therefore performed on the engineering-perturbation layer described below. Exactly four models are compared: the original BP network plus RF, an XGBoost-style regularized second-order tree boosting, and SVR-RBF. In the main benchmark, all four receive the same 11 observable predictors: RAP content, aging degree, rejuvenator dosage, mixing temperature, ambient temperature, aggregate moisture, RAP moisture, plant load, dryer efficiency, dryer-start frequency, and transport multiplier. Complete plant-day blocks are held out in grouped five-fold cross-validation, and R^2, RMSE, MAE, and computational time are reported. A secondary process-only ablation uses only the four process variables to quantify the loss of predictive information when engineering context is unavailable; it is not used as the main model-performance result. Deterministic-grid fitting, if reported, is labeled only as a simulator-surrogate fidelity diagnostic. The structure of the BP neural network is shown in Figure 2.

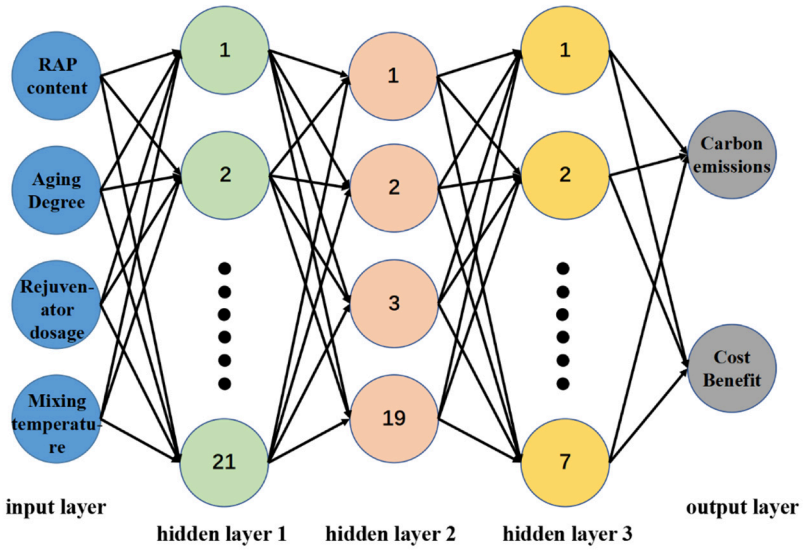


Figure 2. BP neural network model structure.

2.4.1. Engineering-Context Variables and White-Noise Stress Test

To represent engineering variability absent from the full-factorial mechanism dataset, a semi-synthetic observational layer is constructed at plant-day and batch levels. Three hundred plant-day blocks with ten observations per day (3000 observations) are generated. Pre-treatment engineering context includes ambient temperature, aggregate moisture, RAP moisture, plant load/daily production intensity, dryer efficiency, dryer-start frequency, and a transport multiplier. The four process settings are generated conditionally on this context, creating explicit common-cause pathways from engineering background to both process settings and emissions. Continuous settings are restricted to the original design domain and the underlying LCA stage values are linearly interpolated only for this stress-test layer; carbon-only optimization remains grid-supported. Day-level plant heterogeneity and batch-process residuals are then added. Finally, independent Gaussian white measurement noise is superimposed. The main noise standard deviation equals 2% of the mean

context-adjusted emission, rather than 2% of its standard deviation; 0%, 2%, 5%, and 10% of the mean are used in robustness checks. Engineering context is treated as potential observed confounding/background information, whereas white noise represents unresolved stochastic/model-measurement error.

The perturbation ranges are informed by published plant data rather than claimed as measurements from the present project. Schönauer et al. [34] reported about 22% lower fuel consumption per tonne at high versus low daily production and up to 9% fuel saving when mixture temperature decreased from 186 °C to 162 °C. Wang et al. [35], using field measurements from asphalt plants in Anhui, reported for AC-13 approximately 3.623 kWh/t for dust removal, 5.181 kg heavy oil/t for aggregate drying, 1.561 kg natural gas/t for asphalt heating, and 7.302 kWh/t for mixture blending; aggregate drying and asphalt heating accounted for 69.50% and 17.75% of production energy, respectively. Schönauer et al. [36] measured aggregate moisture from 1.46% to 9.83% and found that each 1 mass% increase in moisture added approximately 6.86 kWh/t of dryer energy. These observations are used to define stress-test envelopes and sensitivity coefficients, while parameters without direct project calibration (e.g., RAP-moisture and dryer-start coefficients) remain explicit scenario assumptions.

2.4.2. Four-Model Comparison and Selection of the DML Auxiliary Learner

The predictive comparison includes four models in total: the submitted BP neural network, RF, MATLAB-implemented XGBoost, and SVR-RBF. RF provides a nonparametric bagged-tree ensemble, SVR-RBF provides a kernel-based comparator, and XGBoost provides a regularized boosted-tree comparator [41]. The XGBoost comparator is implemented directly from the regularized second-order boosting objective for squared-error regression. The BP network retains the submitted three-hidden-layer structure (21-19-7) and Bayesian-regularization backpropagation training. All four models receive the same 11 observable predictors and the same plant-day grouped five-fold assignments. After cross-validation, the code ranks the four models by mean R^2 and automatically selects the model with the largest value as the sole auxiliary learner for DML. RMSE and MAE are reported as secondary predictive metrics but do not override the pre-specified R^2 selection rule. Importantly, DML effect estimates are not used to choose the model; this prevents selecting a learner because it produces a preferred causal-effect magnitude or sign.

2.5. Multi-Condition Carbon Emission Prediction and Bayesian Optimization Method

2.5.1. Multi-Condition Carbon Emission Prediction Method

To validate the predictive capability of the model and demonstrate the effects of different parameter combinations, five representative operating conditions were selected as prediction cases. These conditions cover low, medium, and high RAP contents, as well as varying levels of aging, rejuvenator, and temperature, systematically illustrating the trends in carbon emissions. The parameters of the typical operating conditions are shown in Table 5.

Table 5. Typical operating condition parameters.

Case	RAP Content	Aging Degree	Recycling Agent	Temperature (°C)
1	0%	1.0	0%	160
2	30%	1.0	2%	160
3	40%	0.8	1%	140
4	70%	1.6	4%	180
5	90%	1.6	5%	175

2.5.2. Exact-Grid Carbon Screening and Engineering-Constrained Selection

The current main workflow uses exact-grid screening rather than relying on an off-grid Bayesian optimum. First, the minimum life-cycle carbon emission is identified over the complete 21 × 9 × 6 × 9 mechanism grid. Second, a separate engineering-screened candidate is selected from grid points satisfying RAP content of 30–60%, rejuvenator dosage of 1–3%, and mixing temperature of 145–160 °C; the aging coefficient is fixed at 1.0 because aging is treated as a material state rather than a directly adjustable plant control. Both searches minimize modeled carbon emissions only. The engineering-screened solution is therefore a conservative grid-supported low-carbon candidate, not a mechanically validated mixture design; workability, compactability, rutting, cracking, moisture resistance, fatigue, and durability still require laboratory or field verification.

2.6. Causal Inference Analysis Centered on Cross-Fitted DML

The causal target of this study is the model-based intervention effect of changing individual RAP mixture process parameters on life-cycle carbon emissions while controlling for other process variables and observed engineering conditions. The practical increments are defined as RAP content +10 percentage points, aging coefficient +0.1, rejuvenator dosage +1 percentage point, and mixing temperature +10 °C.

For each treatment variable D, the adjustment set Z includes the remaining three process variables and observed engineering-context variables, including ambient temperature, aggregate/RAP moisture, plant load, dryer efficiency, dryer-start frequency, and transport variability. Four machine learning models (BP neural network, RF, XGBoost, and SVR-RBF) are compared using grouped five-fold cross-validation, and the model with the highest mean R^2 is selected as the nuisance learner for cross-fitted DML.

The primary causal estimand is the average intervention effect estimated by cross-fitted DML. Additional analyses, including CATE-style conditional contrasts, mediation analysis, counterfactual analysis, global sensitivity contribution, local marginal-effect analysis, and heterogeneity analysis, are used as mechanism diagnostics to interpret nonlinear responses and parameter interactions within the specified LCA response surface. These analyses are not considered independent evidence of real-world causal effects but are used to support interpretation of the model-based intervention results.

2.6.1. Average Treatment Effect (ATE)

Cross-fitted DML estimates the average intervention effect of each process variable after adjusting for the remaining variables and engineering-context factors. The nuisance functions are estimated through cross-fitting, and the orthogonalized treatment and outcome residuals are used to obtain the effect estimate. The orthogonalized outcome and treatment residuals are then related through the partially linear score in Equation (6).

$$Y - g(Z) = \theta[D - m(Z)] + \varepsilon \quad (6)$$

where Y is the observed engineering-perturbed carbon emission, D is the treatment variable, Z is the adjustment set, $g(Z)$ and $m(Z)$ are cross-fitted nuisance functions, θ is the DML effect per native unit of D, and ε is the residual term.

For engineering interpretation, all effects are reported using fixed practical increments: RAP content +10 percentage points, aging coefficient +0.1, rejuvenator dosage +1 percentage point, and mixing temperature +10 °C. The estimated effects are expressed as t CO_2-eq with corresponding confidence intervals.

2.6.2. Conditional Average Treatment Effect (CATE)

CATE-style analysis evaluates how the modeled RAP effect changes under different combinations of rejuvenator dosage, mixing temperature, and aging coefficient. It is implemented using predefined mechanism-grid conditions and is used to identify condition-dependent emission responses. Equation (7) is the primary formula.

$$CATE_{g(r)} = E_{LCA}(r|z_g) - E_{LCA}(0|z_g) \quad (7)$$

where E_{LCA} is the deterministic mechanism/LCA response, r is RAP fraction, and z_g denotes the fixed rejuvenator–temperature–aging condition for group g.

Five condition groups are used: (1) rejuvenator 0%, 140 °C, aging 0.8 with RAP 10–20%; (2) 1%, 150 °C, aging 1.0 with RAP 25–40%; (3) 2%, 160 °C, aging 1.2 with RAP 45–60%; (4) 3%, 170 °C, aging 1.4 with RAP 65–80%; and (5) 4%, 180 °C, aging 1.6 with RAP 85–100%.

2.6.3. Mediation Effect

Mediation analysis is used to explore the pathway through which rejuvenator dosage affects total carbon emissions. In this study, production-stage carbon emission (E3) is considered as the mediator, and the analysis is interpreted as a pathway diagnostic based on the deterministic LCA response surface.

(1) Total effect model:

$$E = cX + \varepsilon_1 \quad (8)$$

where E is the total carbon emissions; c is the total effect coefficient; and ε_1 is the error term in the total effect model.

(2) Model of the effect of the treatment on the mediator variable:

$$M = aX + \varepsilon_2 \quad (9)$$

where M is the energy consumption during the production stage; a is the path coefficient; and ε_2 is the error term in the model of the treatment's effect on the mediator.

(3) Mediator-outcome model:

$$E = c'X + bM + \varepsilon_3 \quad (10)$$

where E is the total carbon emissions; c' is the direct effect coefficient; b is the coefficient of the effect of the mediator on the outcome; and ε_3 is the error term in the outcome model including the mediator.

The paper decomposition therefore describes how much of the modeled rejuvenator–emission association is aligned with the E3 production-stage pathway under the specified data-generating process.

2.6.4. Counterfactual Prediction

Counterfactual analysis evaluates the modeled emission change caused by modifying one or more process parameters while keeping other conditions unchanged. Exact-grid states are compared to quantify the emission impact of specific process adjustments. Equation (11) is the primary formula.

$$\Delta E_{cf} = E_{LCA}(X_{cf}) - E_{LCA}(X_{base}) \quad (11)$$

where X_{base} is the baseline grid-supported parameter vector; X_{cf} is the counterfactual grid-supported vector; and $E_{LCA}(\cdot)$ is the deterministic mechanism/LCA carbon-emission response.

The baseline is RAP 30%, aging 1.0, rejuvenator 2%, and 160 °C. Three comparisons are evaluated: rejuvenator 2% → 4% at 160 °C, temperature 160 → 150 °C at rejuvenator 2%, and the joint state rejuvenator 4% plus 150 °C.

2.6.5. Global Model-Based Sensitivity Contribution

Global sensitivity contribution analysis evaluates the relative influence of each process variable on the overall variation in the modeled carbon-emission response. The contribution values are calculated from the variation in averaged responses across the parameter levels and are used to identify dominant factors.

$$s_j = SD_l\left\{\text{mean}[E_{LCA}|X_j = x_{j,l}]\right\} \quad (12)$$

$$C_{j_} = 100s_j/\Sigma k_{s_k} \quad (13)$$

Here l indexes the discrete levels of factor j, and k indexes the four process factors.

This metric ranks model-based influence across the deterministic mechanism grid. It is not a Sobol first-order or total-order index and does not decompose interaction variance.

The resulting normalized contributions for RAP content, aging coefficient, rejuvenator dosage, and mixing temperature are used only to prioritize influential model dimensions and to support interpretation of the response surface.

2.6.6. Local Marginal and Interval-Effect Analysis

Local marginal effects are calculated from adjacent points in the deterministic mechanism grid under representative operating conditions. This analysis identifies parameter intervals where small changes produce relatively larger emission variations, as shown in Equation (14).

$$ME_{j,l} = \left[E_{LCA}\left(x_j, l+1\right) - E_{LCA}\left(x_j, l\right)\right]/[x_j, l+1-x_j, l] \times \Delta_j \quad (14)$$

Here Δ_j equals 0.10 for RAP, 0.10 for aging, 0.01 for rejuvenator, and 10 °C for mixing temperature. Both sign and magnitude are retained, and the interval with the largest absolute standardized effect is identified for each factor. These are local response-surface effects rather than global DML estimates.

2.6.7. Model-Based Heterogeneity and Conditional-Contrast Analysis

Heterogeneity analysis evaluates whether the effect of one process adjustment varies under different RAP contents or aging conditions. These conditional contrasts are used to characterize interactions among process variables and identify nonlinear response patterns. These contrasts are defined in Equations (15) and (16).

$$\Delta E_{Rej(r)} = E_{LCA}(r, 1.0, 4\%, 160) - E_{LCA}(r, 1.0, 2\%, 160) \quad (15)$$

$$\Delta E_{RAP(a)} = E_{LCA}(50\%, a, 2\%, 160) - E_{LCA}(30\%, a, 2\%, 160) \quad (16)$$

where r indexes RAP content and a indexes aging coefficient. Positive values indicate higher modeled life-cycle carbon emission after the stated process change.

The purpose is to reveal whether the modeled effect of one process adjustment changes systematically with another process or material condition.

2.7. Cost–Benefit Analysis

To comprehensively evaluate the economic feasibility of different RAP recycling schemes, this study constructs a life-cycle cost–benefit analysis model. The model quantifies costs and savings associated with materials, transport, energy, construction, maintenance, end-of-life treatment, and carbon value. When interpreted together with the LCA results, these indicators reveal whether a carbon-reducing and resource-circular option is also economically supportable under the assumed price conditions. Net benefit and payback-related indicators are therefore used as sustainability decision-support metrics rather than as substitutes for environmental performance.

2.7.1. Cost Composition and Calculation Model

The total cost consists of the following six components, covering the economic inputs of the entire process from raw materials to final disposal, and is calculated according to Equation (17).

$$C_{total} = C_{material} + C_{transport} + C_{energy} + C_{construction} + C_{maintenance} + C_{waste} \quad (17)$$

where C_{total} is the total cost; $C_{material}$ is the material cost; $C_{transport}$ is the transportation cost; C_{energy} is the energy cost; $C_{construction}$ is the construction cost; $C_{maintenance}$ is the maintenance cost; and C_{waste} is the waste disposal cost.

2.7.2. Revenue Composition and Calculation Model

Total revenue comes from material substitution, carbon emission reduction trading, and savings from extended life cycle, and is calculated according to Equation (18).

$$B_{total} = B_{material} + B_{carbon} + B_{maintenance} \quad (18)$$

where B_{total} is the total revenue; $B_{material}$ is the material saving revenue; B_{carbon} is the carbon emission reduction revenue; and $B_{maintenance}$ is the maintenance extension revenue.

2.7.3. Key Economic Evaluation Indicators

(1) Net benefit

Net benefit is a core indicator for evaluating the economic viability of a scheme. It represents the net economic profit generated by the scheme after considering all incremental costs. It answers the question of whether using virgin materials results in a profit or loss compared to adopting the RAP scheme. It is calculated according to Equation (19).

$$B_n = B_{total} - C_{total} - C_{base} \quad (19)$$

where B_n is the net benefit; C_{base} is the total cost of the baseline scheme (0% RAP).

(2) Payback period

The payback period measures how long it takes for the initial additional investment (or cost change) incurred by adopting the RAP technology to be offset by the benefits generated.

3. Results and Discussion

3.1. Four-Model Predictive Benchmark

The main predictive benchmark compares BP, RF, XGBoost, and SVR-RBF using the same 11 observable process-and-context predictors and the same grouped five-fold plant-day partitions. The BP achieved the highest grouped-CV mean R^2 of 0.9638 (RMSE = 12.572 t CO_2-eq; MAE = 9.635 t CO_2-eq), followed by random forest (R^2 = 0.9300; RMSE = 17.501; MAE = 13.428), MATLAB-XGBoost (R^2 = 0.9192; RMSE = 18.790; MAE = 14.388), and SVR-RBF (R^2 = 0.8396; RMSE = 26.576; MAE = 19.650). Figure 3 shows the mean R^2 values and fold-to-fold variability, and Table 6 shows the corresponding out-of-fold predictions. BP was therefore selected automatically as the sole auxiliary nuisance learner for the subsequent DML analysis.

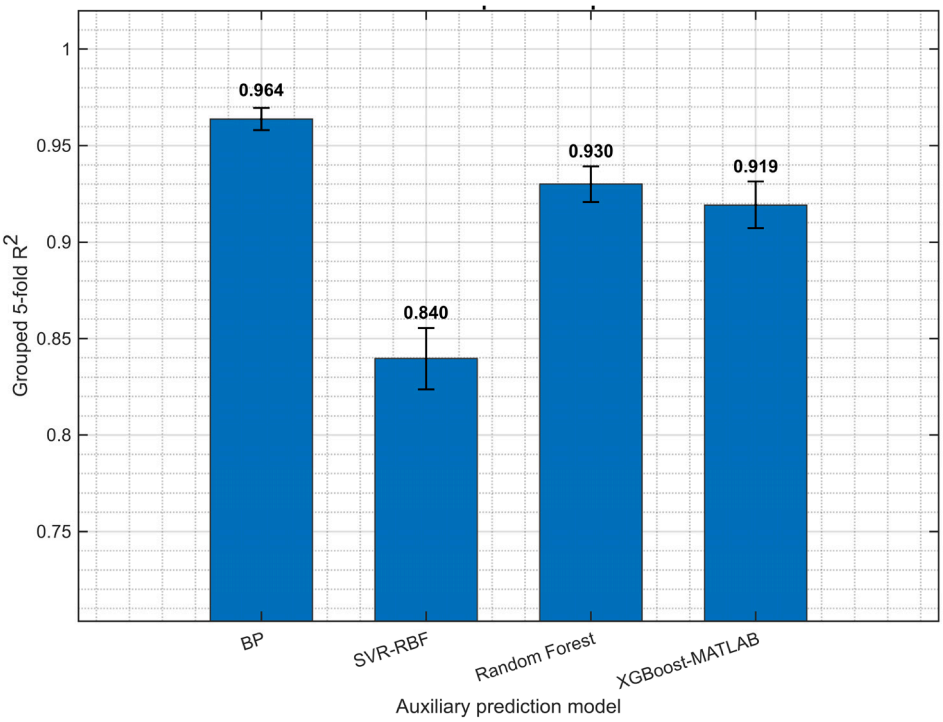


Figure 3. Context-informed grouped five-fold R^2 comparison of BP, SVR-RBF, random forest, and XGBoost.

Table 6. Context-informed four-model predictive benchmark using 11 observable predictors and grouped five-fold cross-validation by plant day.

Model	Mean R^2	Mean RMSE	Mean MAE
BP neural network	0.9638	12.572	9.635
Random forest	0.9300	17.501	13.428
XGBoost	0.9192	18.790	14.388
SVR-RBF	0.8396	26.576	19.650

Best-model selection for causal assistance was based only on the pre-specified criterion of the largest grouped five-fold mean R^2. The selected model was BP ($R^2 = 0.9638$), and neither the sign nor magnitude of the subsequent DML effects was used during model selection.

Figure 3 reports the mean grouped five-fold R^2 of BP, SVR-RBF, random forest, and MATLAB-XGBoost with fold-to-fold standard-deviation error bars.

3.2. Representative Operating Conditions and Exact-Grid Carbon Screening

Representative operating conditions are used for descriptive exact-grid mechanism/LCA comparison. The common reference is 0% RAP, aging 1.0, 0% rejuvenator, and 160 °C, for which the executed model produced 289.557 t CO_2-eq. The remaining four exact-grid cases produced 255.587 t CO_2-eq (−11.73%) for 30% RAP/1.0 aging/2% rejuvenator/160 °C; 216.259 t CO_2-eq (−25.31%) for 40% RAP/0.8 aging/1% rejuvenator/140 °C; 553.691 t CO_2-eq (+91.22%) for 70% RAP/1.6 aging/4% rejuvenator/180 °C; and 596.342 t CO_2-eq (+105.95%) for 90% RAP/1.6 aging/5% rejuvenator/175 °C. All percentage changes in Table 7 use the same reference.

Table 7. LCA/model results under representative grid-supported operating conditions.

Case	RAP Content	Aging Degree	Recycling Agent	Temperature	Predicted Carbon Emission	Change Relative to Baseline
1	0%	1.0	0%	160 °C	289.557	0.00%
2	30%	1.0	2%	160 °C	255.587	−11.73%
3	40%	0.8	1%	140 °C	216.259	−25.31%
4	70%	1.6	4%	180 °C	553.691	+91.22%
5	90%	1.6	5%	175 °C	596.342	+105.95%

The executed workflow produced two exact-grid carbon-screening results. The unrestricted grid minimum was 186.672 t CO_2-eq at 50% RAP, aging 0.8, 0% rejuvenator, and 140 °C, which is 35.53% below the 289.557 t CO_2-eq reference. Under the conservative engineering screen (RAP 30–60%, rejuvenator 1–3%, temperature 145–160 °C, aging fixed at 1.0), the minimum was 215.278 t CO_2-eq at 50% RAP, 1% rejuvenator, and 145 °C, corresponding to a 25.65% reduction. Both are exact grid points; no off-grid interpolation is used for these reported screening results.

$$E_{min} = \min_{\{x \in G\}} E_{LCA(x)} \quad (20)$$

where G is either the full mechanism grid or the engineering-screened subset and $E_{LCA(x)}$ is the directly calculated life-cycle carbon emission at grid point x.

The unrestricted minimum is a mathematical carbon-only lower bound and should not be interpreted as an engineering mixture recommendation. The engineering-screened candidate uses conservative process bounds but still lacks laboratory/field performance constraints; its mechanical feasibility therefore requires independent verification.

3.3. DML Causal-Effect Analysis and Secondary Mechanism Diagnostics

All effects in this section are interpreted within the specified LCA/engineering-perturbation data-generating process. The primary causal estimand is the cross-fitted DML practical-increment effect under the stated adjustment assumptions. The other six analyses—CATE-style conditional contrasts, mediation, counterfactuals, global model-based sensitivity contribution, finite-difference marginal effects, and heterogeneity—are secondary mechanism diagnostics. Their conditioning sets and units differ from the global DML result and they are not presented as independent proof of real-world causal effects.

3.3.1. Cross-Fitted DML Using the Best-Performing Model Selected from the Four-Model Benchmark

The four predictive models were compared first, and BP was carried into the causal stage because it had the highest grouped-CV mean R^2 (0.9638). The BP model family was used for both outcome and treatment nuisance learning within plant-day cross-fitting. For computational efficiency, the repeated nuisance fits used the pre-specified reduced-complexity BP configuration while retaining the same selected model family. The executed run used four parallel workers and reused the existing audited DML cache when available.

Effects are reported on common practical increments. Cross-fitted DML effect estimates result in Table 8. The executed DML estimates were: RAP + 10 percentage points, 12.492 t CO_2-eq (SE = 1.388; 95% CI: 9.770–15.213); aging + 0.1, 7.077 t CO_2-eq (SE = 0.422; 95% CI: 6.250–7.904); rejuvenator + 1 percentage point, 13.189 t CO_2-eq (SE = 0.451; 95% CI: 12.306–14.073); and mixing temperature + 10 °C, 8.632 t CO_2-eq (SE = 0.739; 95% CI: 7.182–10.081). All four estimates use BP as the selected nuisance learner.

Table 8. Cross-fitted DML effect estimates using the best-performing model selected from the four-model grouped-CV benchmark.

Treatment	Reporting Increment	Selected Best Model	DML Effect (t CO_2-eq)	95% CI (t CO_2-eq)
RAP content	+10 percentage points	BP	12.492	9.770 to 15.213
Aging coefficient	+0.1	BP	7.077	6.250 to 7.904
Rejuvenator dosage	+1 percentage point	BP	13.189	12.306 to 14.073
Mixing temperature	+10 °C	BP	8.632	7.182 to 10.081

Figure 4 presents the four selected-model DML estimates as a forest plot. Each row corresponds to one practical process increment and shows the estimated intervention effect with its 95% confidence interval and a zero-effect reference line. Because model selection occurs before DML and is based only on grouped-CV predictive accuracy, Figure 4 visualizes the causal target after the auxiliary-learning decision rather than comparing causal results across algorithms. Different colors distinguish the four intervention estimates in Figure 4.

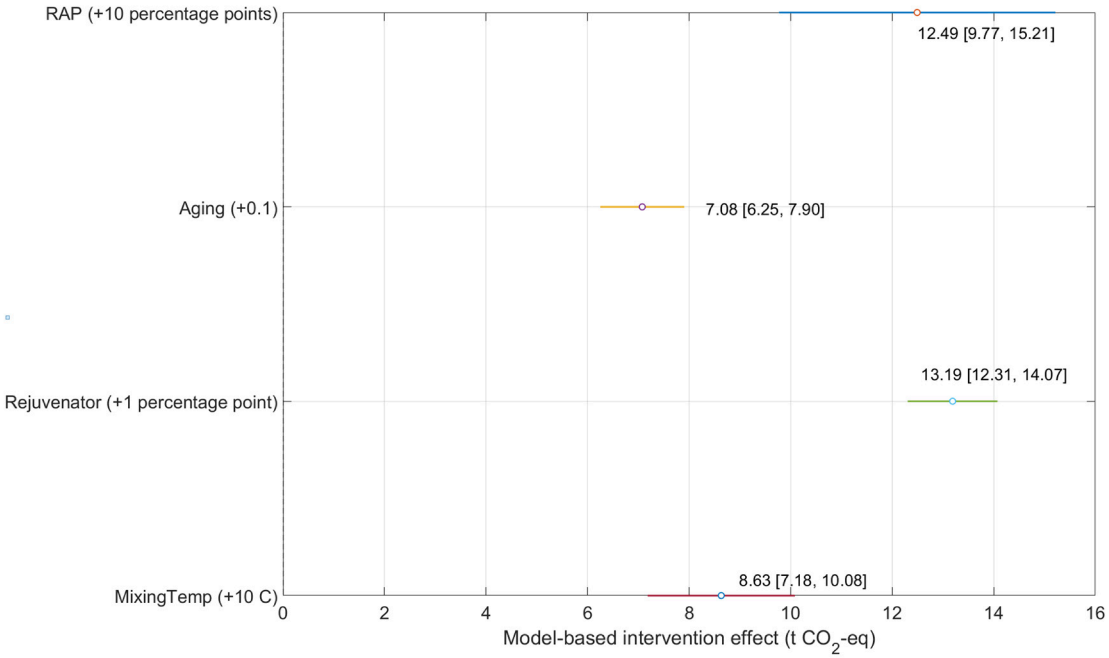


Figure 4. Cross-fitted DML practical-increment effects using the automatically selected best-performing prediction model as the sole nuisance learner.

3.3.2. Secondary Diagnostics

Marginal-effect and heterogeneity analyses complement the global DML estimand by asking how the modeled response changes locally and whether the effect of one process adjustment varies with the level of another factor. In causal-inference terms, these analyses are useful for detecting nonlinearity and effect modification that can be hidden by an average treatment effect. They are therefore important for translating the global DML result into condition-specific engineering interpretation, although in this study they remain diagnostics of the programmed LCA response surface rather than separately identified field-causal estimands. Figures 5 and 6 present the corresponding local and conditional patterns.

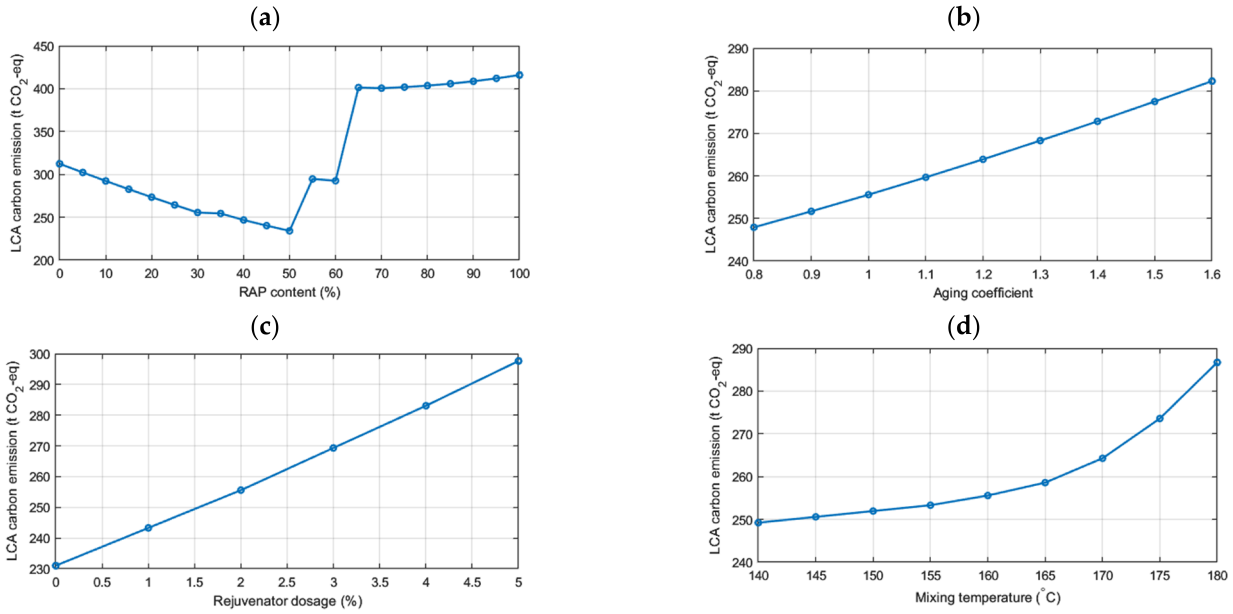


Figure 5. Mechanism-based one-factor response curves: (**a**) RAP content; (**b**) aging coefficient; (**c**) rejuvenator dosage; (**d**) mixing temperature.

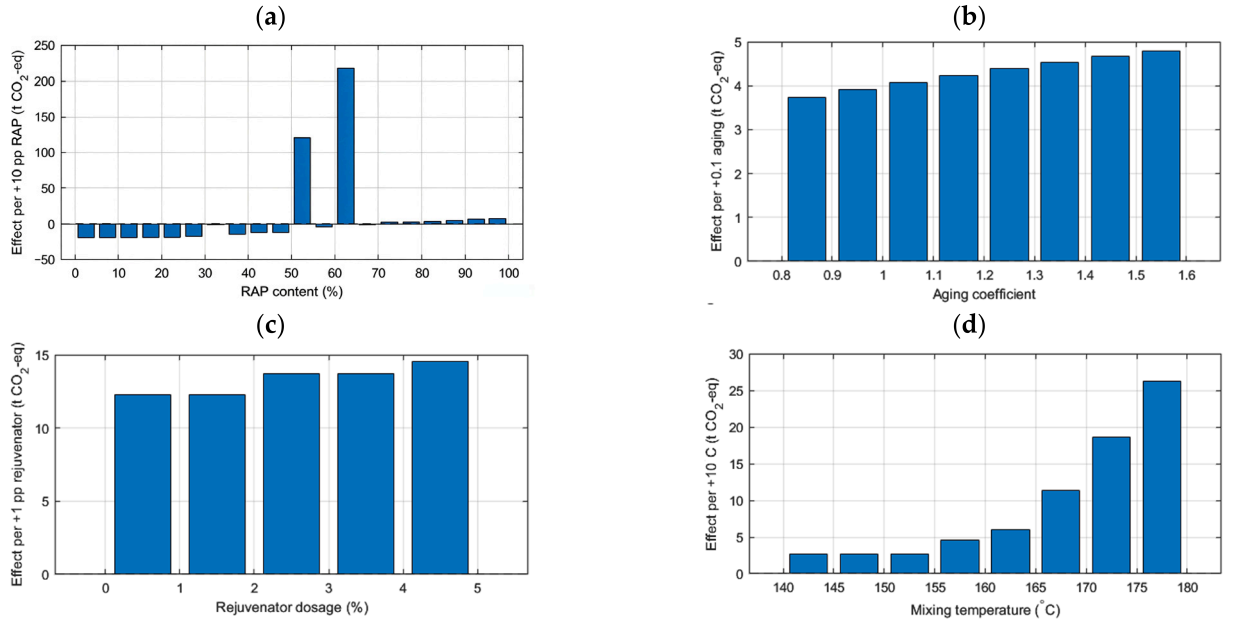


Figure 6. Signed local finite-difference effects: (**a**) RAP content; (**b**) aging coefficient; (**c**) rejuvenator dosage; (**d**) mixing temperature.

Figures 5 and 6 show pronounced nonlinearity in the modeled RAP response. The carbon-emission response decreases over much of the low-to-moderate RAP range and then changes sharply in the higher-RAP region. The largest absolute standardized local effect occurs at RAP 60–65%, reaching 217.582 t CO_2-eq per +10-percentage-point RAP increment. The strongest local intervals for aging, rejuvenator dosage, and mixing temperature are 1.5–1.6 (4.800 t CO_2-eq per + 0.1), 4–5% (14.574 t CO_2-eq per + 1 percentage point), and 175–180 C (26.219 t CO_2-eq per + 10 C), respectively. These results show that the modeled process response is not well represented by a constant slope across the full factor range. The practical significance is that the global DML effect should be interpreted as an average intervention effect, while threshold-like regions, especially the RAP 60–65% interval and

high-temperature range, require separate attention because small parameter changes there can produce much larger modeled emission responses.

Figure 7 further demonstrates conditional effect heterogeneity. Increasing rejuvenator dosage from 2% to 4% at aging 1.0 and 160 C increases modeled life-cycle emissions by 26.843–28.528 t CO_2-eq as RAP varies from 10% to 90%, indicating a consistently positive emission penalty over the examined RAP range. In contrast, the effect of increasing RAP from 30% to 50% at 2% rejuvenator and 160 C varies from −27.966 to +1.222 t CO_2-eq as the aging coefficient rises from 0.8 to 1.6. Thus, the modeled carbon benefit of additional RAP is substantial at low aging levels but diminishes and approaches a sign reversal as aging becomes more severe. This is important for causal interpretation because a single average effect can conceal condition-dependent changes in both magnitude and direction. Engineering decisions on RAP content should therefore be conditioned on material state and accompanying process settings rather than based on a universal RAP target.

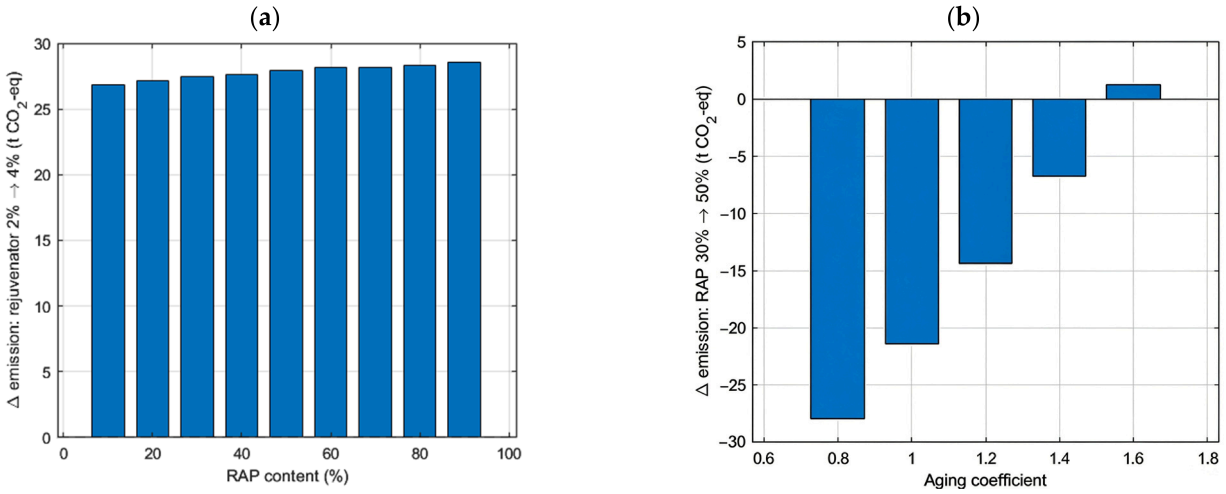


Figure 7. Model-based conditional-contrast diagnostic analogous to the original heterogeneity plots: (**a**) emission change for rejuvenator 2% → 4% across RAP levels at aging 1.0 and 160 °C; (**b**) emission change for RAP 30% → 50% across aging levels at rejuvenator 2% and 160 °C.

3.4. Engineering Perturbation, White-Noise Robustness, and Extended Mechanism Diagnostics

Causal interpretation is useful only when the estimated effects remain reasonably stable under plausible engineering perturbations and when their conditional patterns and limits of transportability are understood. This section therefore evaluates outcome-noise robustness, conditional RAP effects, mediation and counterfactual structure, global response sensitivity, and the Sim-to-Real boundary. These analyses do not replace the primary cross-fitted DML estimator; instead, they test the stability, mechanism interpretation, and practical relevance of the model-based causal conclusions. The engineering layer contains 300 plant-day blocks and 3000 observations, with a main Gaussian white-noise standard deviation of 6.54 t CO_2-eq, equal to 2.0% of the mean context-adjusted outcome.

3.4.1. White-Noise Robustness of the Selected-Model DML Effects

In causal inference, an estimated intervention effect is more credible when its direction and approximate magnitude are not driven by modest outcome noise. White-noise stress testing is therefore used here as a robustness diagnostic for the cross-fitted DML estimates. It evaluates sensitivity to unresolved measurement or model error while retaining BP as the selected nuisance-model family; in the fast configuration, the cached cross-fitted nuisance predictions are held fixed so that the comparison isolates alternative outcome-noise realizations. The 0%, 2%, 5%, and 10% noise scenarios are shown in Figure 8.

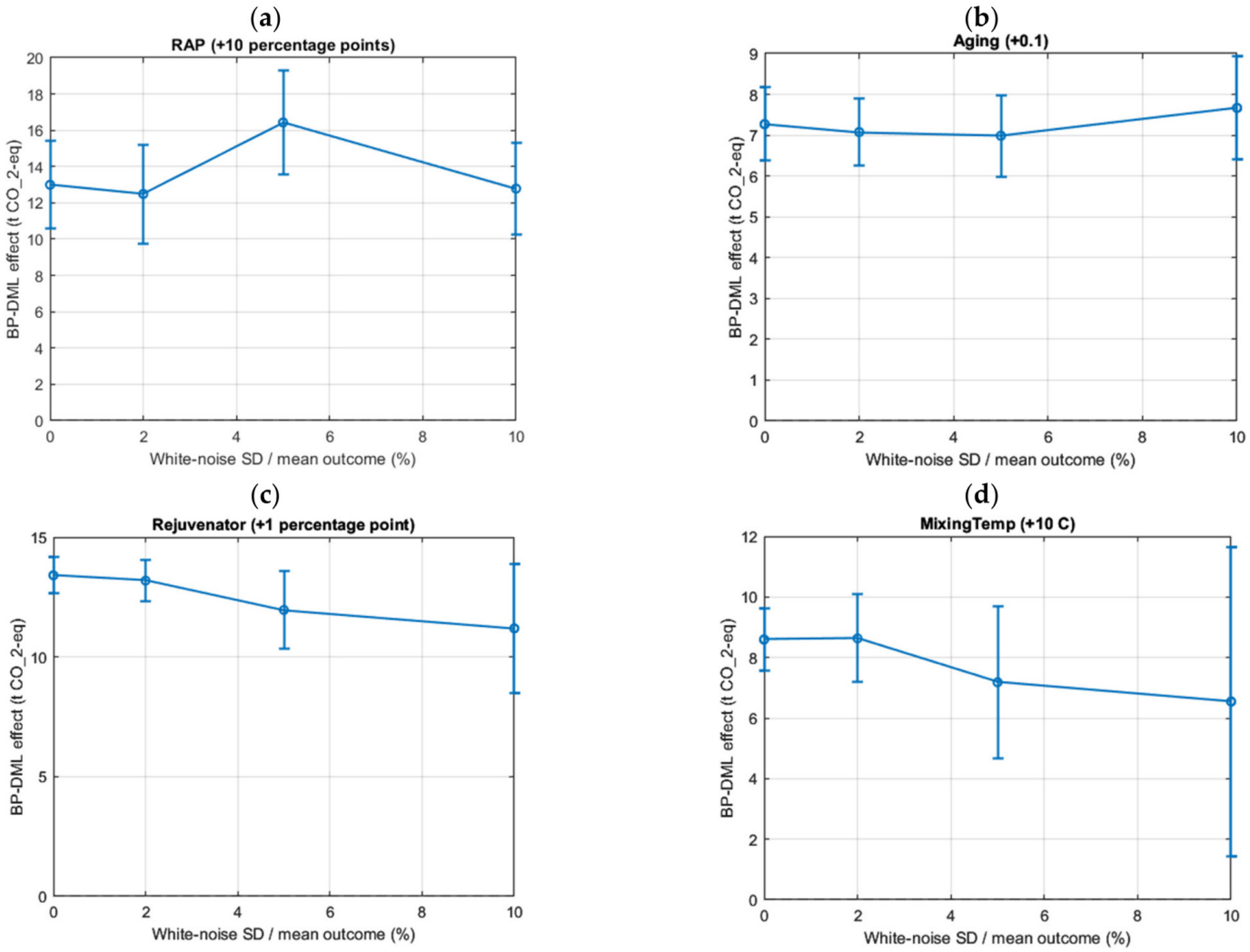


Figure 8. Fast fixed-nuisance robustness of the selected-model DML practical-increment effects to additive Gaussian white noise with standard deviations of 0%, 2%, 5%, and 10% of the mean context-adjusted carbon emission. (**a**) RAP content; (**b**) aging coefficient; (**c**) rejuvenator dosage; (**d**) mixing temperature.

Figure 8 indicates that the four DML effect estimates preserve their positive direction across all examined white-noise levels, and the displayed 95% confidence intervals remain above the zero-effect reference. The aging effect is comparatively stable, whereas the RAP estimate shows greater fluctuation and the rejuvenator and mixing-temperature estimates tend to decline as stronger noise is introduced. Confidence intervals also become wider at the higher-noise settings, particularly for the temperature effect. The significance of this result is that the main directional DML conclusions are not produced by a single low-noise realization, although the magnitude of some effects is more noise-sensitive than others. This robustness test should not be interpreted as proof against unmeasured confounding, because the perturbation acts on the outcome and the fast configuration keeps the nuisance predictions fixed; rather, it is evidence of stability to the specified measurement-noise stress test.

3.4.2. CATE-Style Conditional RAP Contrasts

Conditional average treatment effect analysis is intended to reveal whether an intervention has different consequences under different background conditions. This is important because a global average effect may hide subgroups in which the magnitude or even the

direction of the response changes. In the present study, CATE-style exact-grid contrasts compare selected RAP levels with RAP = 0 under five representative combinations of rejuvenator dosage, mixing temperature, and aging coefficient. The resulting conditional patterns are shown in Figure 9; they are interpreted as mechanism-surface diagnostics rather than independently identified field CATEs.

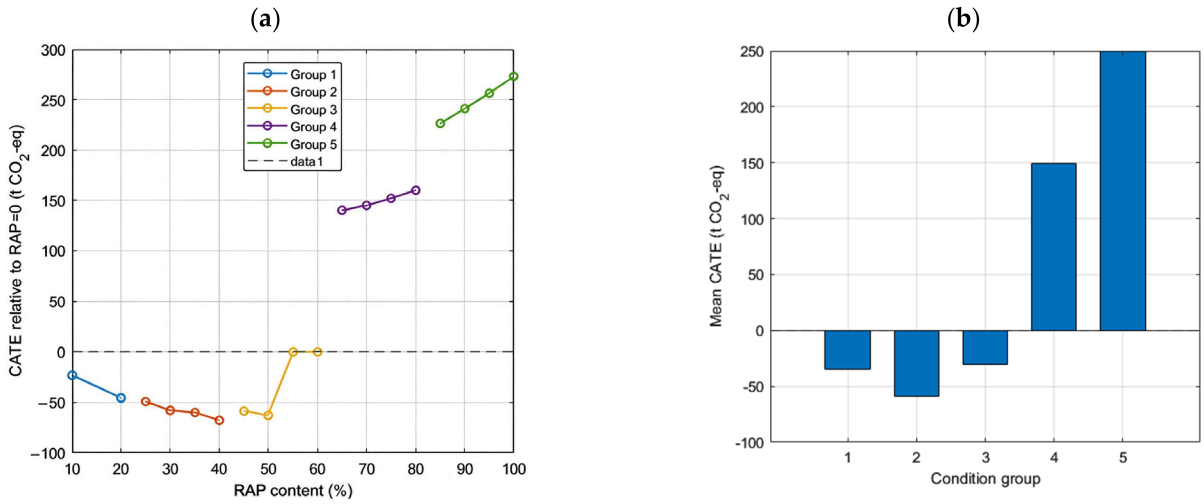


Figure 9. CATE-style conditional RAP contrasts relative to RAP = 0 under five representative rejuvenator–temperature–aging conditions: (**a**) contrast versus RAP content within each condition group; (**b**) mean CATE-style contrast by condition group.

Figure 9 shows a clear transition across the five condition groups. The mean contrasts are −34.412 t CO_2-eq for Group 1, −58.598 t CO_2-eq for Group 2, and −30.466 t CO_2-eq for Group 3, indicating lower modeled emissions than the RAP = 0 reference under these lower-to-moderate condition combinations. In contrast, Group 4 and Group 5 show positive mean contrasts of +149.262 and +249.251 t CO_2-eq, respectively. The change from negative to strongly positive contrasts indicates that the modeled environmental benefit of RAP is highly condition-dependent and can turn into an emission penalty under more adverse combinations of aging, temperature, and rejuvenator dosage. This is important for causal interpretation because it demonstrates why the global DML ATE should not be translated into a one-size-fits-all RAP recommendation. Because the three conditioning variables change together across the predefined groups, however, the sign change cannot be attributed to any single modifier in isolation.

3.4.3. Mediation and Counterfactual Mechanism Diagnostics

Mediation and counterfactual analyses address two complementary causal questions. Mediation analysis examines the pathway through which an exposure is associated with the outcome. Counterfactual analysis estimates the modeled outcome that would be expected under a specified intervention while other factors are held fixed. These questions are important because an average effect estimate alone does not reveal the operating pathway or the consequence of a concrete process change. In this study, mediation is treated as a pathway decomposition on the deterministic mechanism grid, while the counterfactual analysis uses exact-grid intervention contrasts. Figure 10 presents both diagnostics.

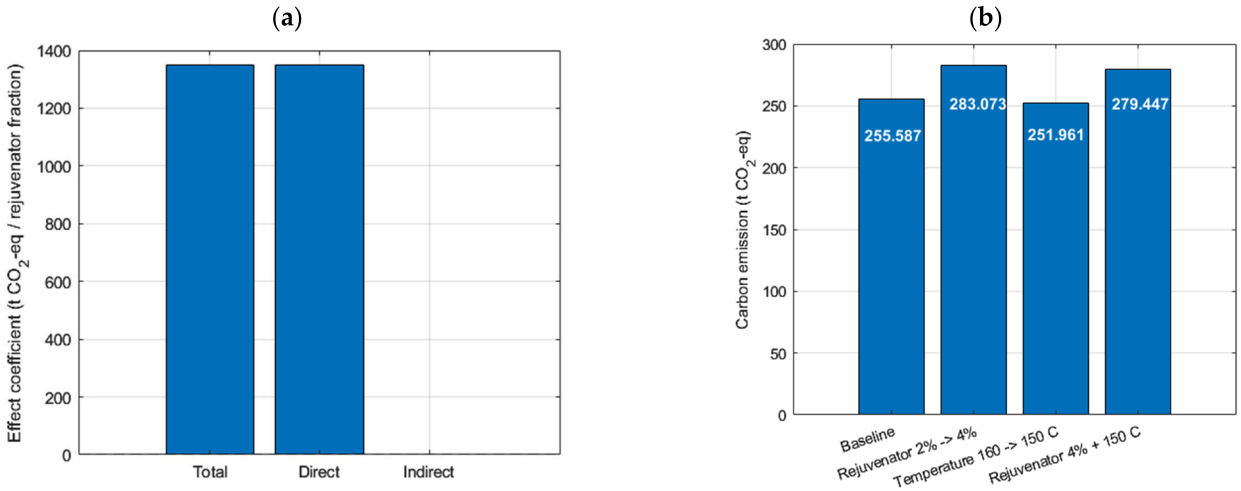


Figure 10. Secondary mechanism diagnostics: (**a**) rejuvenator-to-E3 mediation decomposition into total, direct, and indirect components; (**b**) exact-grid counterfactual carbon emissions for the baseline and three specified process-change scenarios.

In Figure 10a, the rejuvenator-to-E3-to-total-emission decomposition yields a total coefficient of 1349.9229 t CO_2-eq per rejuvenator fraction, a direct coefficient of 1349.9229, an indirect coefficient of 0.0000, and a mediation proportion of 0.00%. Under the current linear decomposition, the selected E3 pathway therefore does not explain an additional indirect component of the modeled rejuvenator–emission relationship; the estimated association is entirely assigned to the direct component relative to this mediator specification. Figure 10b provides the complementary intervention perspective. Starting from the exact-grid baseline of 255.587 t CO_2-eq, increasing rejuvenator dosage from 2% to 4% raises emissions to 283.073 t CO_2-eq (+10.75%), reducing temperature from 160 C to 150 C lowers emissions to 251.961 t CO_2-eq (−1.42%), and combining 4% rejuvenator with 150 C produces 279.447 t CO_2-eq (+9.34%). Thus, the carbon saving from the lower temperature is insufficient to offset the increase associated with the higher rejuvenator dosage in this baseline state. The significance is that intervention decisions should be evaluated jointly rather than assuming that one favorable adjustment will necessarily compensate for another unfavorable one.

3.4.4. Global Sensitivity Results

Global sensitivity analysis is not itself a causal-effect estimator, but it is an important complement to causal inference because it identifies which modeled inputs account for the greatest overall variation in the response surface. Such information helps prioritize measurement quality, process control, and the variables for which effect heterogeneity deserves closer examination. The present metric is the normalized variability of level-wise mean mechanism responses, not a Sobol variance decomposition. Figure 11 summarizes the resulting global contributions.

Figure 11 shows that RAP content contributes 55.35% of the normalized global response variability, making it the dominant factor over the modeled design space. Rejuvenator dosage contributes 17.07%, aging coefficient 16.49%, and mixing temperature 11.09%. The result highlights RAP as the factor that most strongly structures the overall response surface and therefore as the highest-priority dimension for global process monitoring and condition-specific analysis. Importantly, these percentages should not be equated with the DML practical-increment effects. For example, rejuvenator has a DML effect of 13.189 t CO_2-eq per + 1 percentage point, slightly larger than the 12.492 t CO_2-eq effect for RAP + 10 percentage points, even though its global sensitivity contribution is much smaller. This

distinction is important: sensitivity ranks response variability over the full factor range, whereas DML estimates the average intervention effect on a specified practical increment.

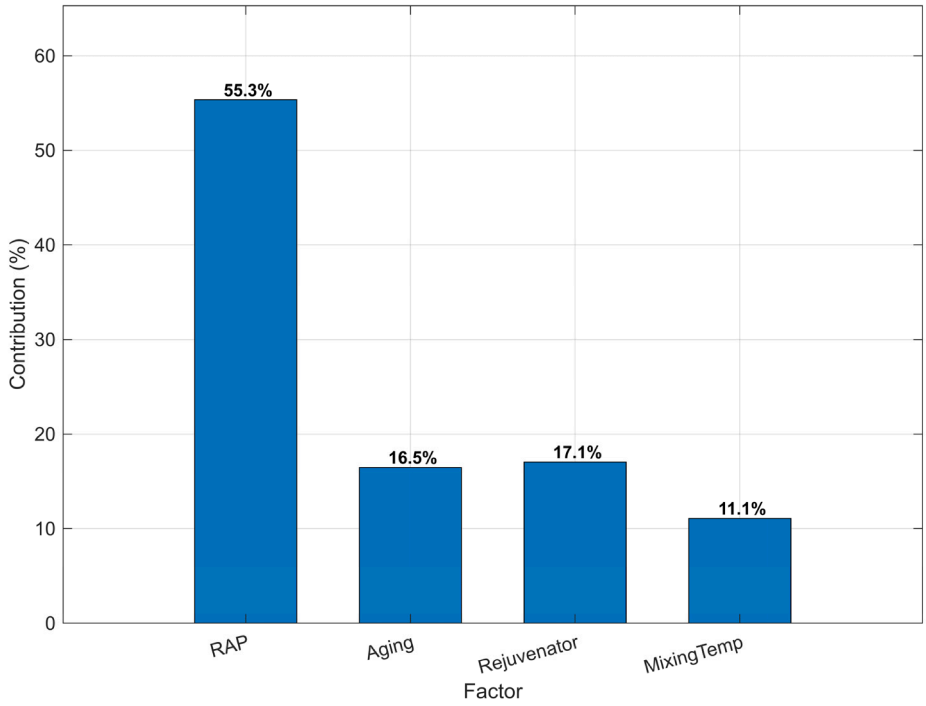


Figure 11. Model-based global sensitivity contribution of RAP content, aging coefficient, rejuvenator dosage, and mixing temperature.

3.4.5. External Engineering Evidence and Sim-to-Real Boundary

External evidence is directly related to the transportability and external-validity stage of causal inference. An effect can be internally well defined within a model-based data-generating process yet still fail to transfer to real plants if the operating ranges, energy pathways, or disturbance structure are unrealistic. Published plant and project data are therefore used here to check engineering scale and plausible perturbation directions, not as sample-level validation of the complete LCA model.

The published evidence supports the order of magnitude and direction of several engineering perturbations used in the study. Schönauer et al. (2024) [34] reported approximately 22% lower fuel consumption per tonne at high production volume and up to 9% fuel saving when production temperature decreased from 186 C to 162 C. Wang et al. (2024) [35] reported 3.623 kWh/t for dust removal, 5.181 kg heavy oil/t for aggregate drying, 1.561 kg natural gas/t for asphalt heating, and 7.302 kWh/t for blending in AC-13 production. Schönauer et al. (2026) [36] measured aggregate moisture of 1.46–9.83% and approximately 6.86 kWh/t additional dryer energy per 1 mass% moisture increase. Additional plant and project studies provide comparable energy and carbon-emission scales but use different system boundaries and mixture conditions. The significance of these comparisons is that they support the plausibility of the stress-test layer while also defining a clear Sim-to-Real boundary: the present results remain model-based until project-specific records with the same 11 observable predictors and measured carbon emissions are available for true external validation.

3.5. Grid-Supported Carbon Screening and Engineering-Screened Low-Carbon Candidate

Carbon screening is a downstream decision-support step rather than a separate causal estimator. Its relationship to the causal analysis is that the estimated intervention patterns

and mechanism diagnostics are translated into candidate operating combinations on the same LCA response surface. This step is important because causal-effect estimation is most useful when it can inform a practical decision while clearly separating a mathematical carbon minimum from a more conservative engineering-screened choice. Figure 12 compares the reference condition, the unrestricted grid minimum, and the engineering-screened candidate.

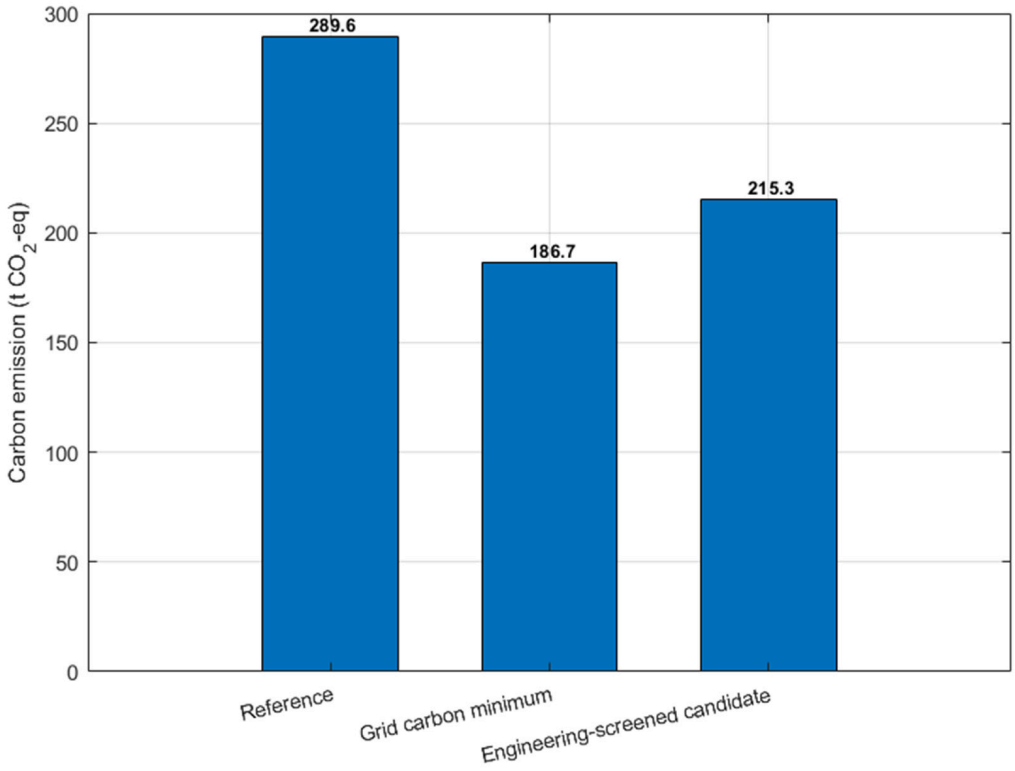


Figure 12. Comparison of the reference condition, the unrestricted grid-supported carbon minimum, and the engineering-screened low-carbon candidate.

Figure 12 shows a reference emission of 289.557 t CO_2-eq. The unrestricted 10,206-case grid minimum is 186.672 t CO_2-eq at 50% RAP, aging 0.8, 0% rejuvenator, and 140 C, corresponding to a 35.53% reduction from the reference. After applying the conservative screen of RAP 30–60%, rejuvenator 1–3%, mixing temperature 145–160 C, and aging fixed at 1.0, the lowest-emission candidate is 215.278 t CO_2-eq at 50% RAP, 1% rejuvenator, and 145 C, corresponding to a 25.65% reduction. The engineering screen therefore gives up 28.606 t CO_2-eq of the theoretical carbon advantage, or 9.88 percentage points of reduction relative to the reference, in exchange for remaining within the pre-specified conservative process window. The result is consistent with the preceding causal and mechanism diagnostics: RAP is the dominant global response dimension, but its effect is nonlinear and condition-dependent, so the lowest-carbon decision cannot be inferred from RAP content alone. The screened solution should still be regarded as a carbon-only candidate, because workability, compaction, rutting, moisture resistance, cracking, fatigue, durability, and field performance have not been experimentally validated in the present dataset.

3.6. Results of Cost–Benefit Analysis of the Carbon Emission Model

Cost–benefit analysis is the final decision-support layer of the causal analysis framework. It does not provide an additional causal estimand; instead, it tests whether the low-carbon operating combination selected after the intervention and mechanism analyses remains economically attractive when the same life-cycle cost equations are applied. This

step is important because an intervention can reduce carbon emissions while increasing material or energy expenditure, so carbon optimality and economic optimality should not be assumed to coincide. Figure 13 retains the two most decision-relevant outputs from the executed cost–benefit module: the RAP-dependent cost/economic-effect curve and the cost composition of the engineering-screened candidate.

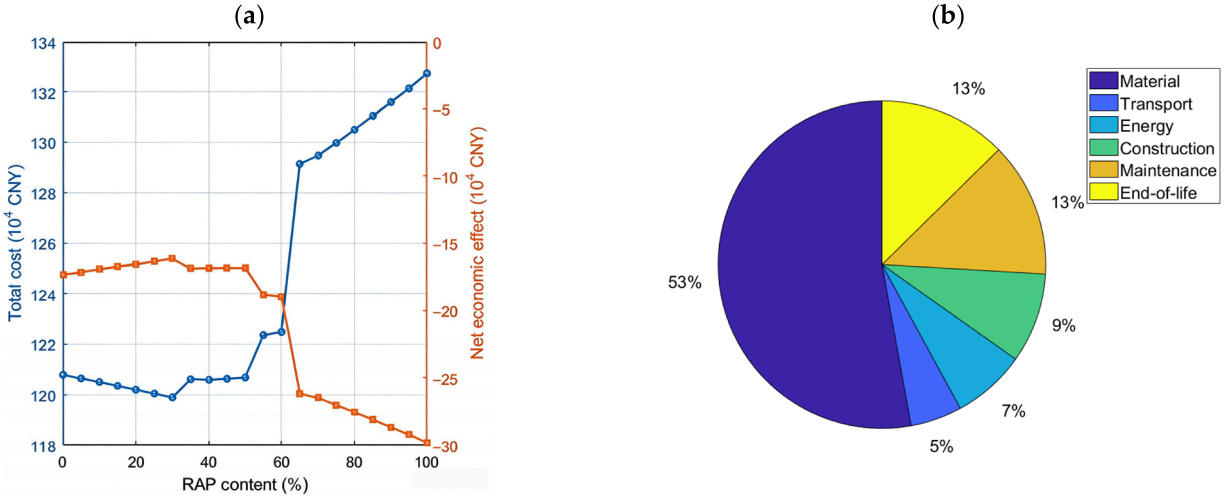


Figure 13. Selected outputs from the audited life-cycle cost–benefit analysis: (**a**) RAP content versus total life-cycle cost and net economic effect; (**b**) cost composition of the engineering-screened candidate.

Figure 13a shows the one-factor RAP sweep with aging fixed at 1.0, rejuvenator at 2%, and mixing temperature at 160 °C. The modeled total life-cycle cost decreases slightly from 0% to about 30% RAP, remains near its low level through the moderate-RAP range, and then increases sharply once RAP exceeds about 60%. The net economic effect remains negative throughout the sweep and becomes markedly more unfavorable beyond the same high-RAP region. This pattern indicates a nonlinear economic response and reinforces that increasing RAP cannot be evaluated from carbon reduction alone: high RAP can introduce a substantial cost penalty even when environmental benefits are considered.

Figure 13b shows that the engineering-screened candidate is dominated by material cost (53% of total modeled life-cycle cost), followed by maintenance (13%), end-of-life treatment (13%), construction (9%), energy (7%), and transportation (5%). For the selected candidate (50% RAP, aging 1.0, 1% rejuvenator, and 145 °C), the executed model gives a total cost of 109.65×10^4 CNY compared with 103.55×10^4 CNY for the reference, an increase of 6.10×10^4 CNY. Its 74.278 t CO_2-eq reduction is valued at only 0.371×10^4 CNY at 50 CNY/t CO_2-eq, giving a net economic effect of -5.729×10^4 CNY and a break-even carbon price of approximately 821 CNY/t CO_2-eq. This divergence is a central sustainability result: the selected scheme improves environmental performance and material circularity but is not cost-saving under the present market assumptions. Sustainable implementation would therefore require either lower material/rejuvenator costs, a higher effective value of avoided carbon, other unmodeled benefits, or a different process configuration. Because materials account for more than half of modeled total cost, procurement and rejuvenator-price control are particularly influential. These economic conclusions remain scenario-dependent and should be re-evaluated using project-specific procurement, energy, maintenance, end-of-life, and carbon-price data before engineering adoption.

4. Conclusions

Sustainable use of RAP requires more than increasing recycled content or minimizing a single carbon indicator. It requires a life-cycle view that connects circular resource use, greenhouse-gas reduction, engineering uncertainty, causal process understanding, and economic feasibility. To address these interacting dimensions, this study integrates LCA, a thermodynamic mechanism model, four machine learning models, selected-model-assisted cross-fitted DML, mechanism diagnostics, engineering-constrained low-carbon screening, and life-cycle cost–benefit analysis. Based on the 10,206-point deterministic LCA mechanism grid and a 3000-observation semi-synthetic plant-day layer, the framework links predictive benchmarking, model-based causal-effect estimation, circular-material/carbon screening, and environmental–economic evaluation within a unified sustainability-oriented workflow. The main conclusions are as follows:

(1) Under the same context-informed plant-day grouped five-fold validation, BP achieved the highest predictive accuracy ($R^2 = 0.9638$) and was therefore selected automatically as the nuisance learner for cross-fitted DML. The estimated practical-increment effects were 12.492 t CO_2-eq for RAP + 10 percentage points, 7.077 t CO_2-eq for aging + 0.1, 13.189 t CO_2-eq for rejuvenator + 1 percentage point, and 8.632 t CO_2-eq for mixing temperature + 10 °C; all effects remained positive in the 0–10% white-noise robustness tests.

(2) The mechanism diagnostics reveal pronounced nonlinearity and condition dependence. RAP contributed the largest normalized global response share (55.35%) and showed a strong local response around 60–65% RAP. CATE-style, heterogeneity, counterfactual, mediation, and marginal analyses further indicate that RAP effects depend jointly on aging, rejuvenator dosage, and mixing temperature rather than on RAP content alone.

(3) The unrestricted grid minimum was 186.672 t CO_2-eq at 50% RAP, aging 0.8, 0% rejuvenator, and 140 °C, representing a 35.53% reduction from the reference. After applying the conservative engineering window, the selected candidate was 50% RAP, aging 1.0, 1% rejuvenator, and 145 °C, with 215.278 t CO_2-eq and a 25.65% reduction, demonstrating the distinction between a mathematical carbon minimum and an engineering-screened low-carbon solution.

(4) The engineering-screened candidate increased modeled life-cycle cost by 6.10×10^4 CNY and produced a net economic effect of -5.729×10^4 CNY at a carbon value of 50 CNY/t CO_2-eq; the estimated break-even carbon price was about 821 CNY/t CO_2-eq. Thus, carbon reduction does not necessarily imply economic optimality. Because the analysis remains based on the programmed LCA framework and semi-synthetic engineering perturbations, project-specific emissions, local costs, and laboratory/field performance should be validated before practical implementation.

Author Contributions: Conceptualization, M.R.; methodology, M.R.; software, M.R.; validation, X.L.; formal analysis, X.L.; investigation, X.L.; resources, J.G.; data curation, J.G.; writing—original draft preparation, Z.P.; writing—review and editing, Z.P.; visualization, L.W.; supervision, L.W.; project administration, L.W.; funding acquisition, M.R. All authors have read and agreed to the published version of the manuscript.

Funding: Natural Science Foundation of Inner Mongolia Autonomous Region (Grant No. 2024QN05024).

Data Availability Statement: Data will be made available on request.

Acknowledgments: The authors are grateful for the financial support provided by the Natural Science Foundation of Inner Mongolia Autonomous Region (Grant No. 2024QN05024).

Conflicts of Interest: Author Xin Luo and Jian Gao has received research grants from Company Inner Mongolia Transportation Group Mengtong Maintenance Co., Ltd. The other authors declare no conflict of interest.

References

1. Liu, X.; Deng, L.; Zhang, H.; Yu, J. Quantitative study on carbon emissions of modified recycled asphalt mixture based on life cycle assessment method. *Dev. Built Environ.* **2024**, *20*, 100584. [CrossRef]
2. Mao, J.; Zhu, Y.; Chen, Q.; Yu, H. Energy consumption and carbon emission analysis of typical regeneration methods for asphalt pavements. *Buildings* **2023**, *13*, 1569. [CrossRef]
3. Rafiq, W.; Musarat, M.A.; Altaf, M.; Napiah, M.; Sutanto, M.H.; Alaloul, W.S.; Javed, M.F.; Mosavi, A. Life Cycle Cost Analysis Comparison of Hot Mix Asphalt and Reclaimed Asphalt Pavement: A Case Study. *Sustainability* **2021**, *13*, 4411. [CrossRef]
4. Calabi-Floody, A.T.; Valdés-Vidal, G.A.; Sanchez-Alonso, E.; Mardones-Parra, L.A. Evaluation of Gas Emissions, Energy Consumption and Production Costs of Warm Mix Asphalt (WMA) Involving Natural Zeolite and Reclaimed Asphalt Pavement (RAP). *Sustainability* **2020**, *12*, 6410. [CrossRef]
5. Wang, J.; Sha, C.; Ly, S.; Wang, H.; Sun, Y.; Guo, M. Life Cycle Carbon Emissions and an Uncertainty Analysis of Recycled Asphalt Mixtures. *Sustainability* **2023**, *15*, 16368. [CrossRef]
6. Liu, M.; Luo, S.; Huang, W.; Yang, Y.; Hu, J.; Zhang, Z.; Zhang, B.; Du, K. Enabling high-RAP-content recycling in asphalt pavements through epoxy modification: Durability and life cycle assessment. *Sustain. Mater. Technol.* **2025**, *45*, e01519. [CrossRef]
7. Li, M.; Liu, L.; Han, Z.; Cheng, H.; Xing, C.; Hu, Y. Impact of Production Temperatures on Blending Condition between Virgin and Aged Asphalt: Performance and Environmental Cost Analysis. *J. Mater. Civ. Eng.* **2026**, *38*, 04025604. [CrossRef]
8. Zhang, K.; Huchet, F.; Hobbs, A. A review of thermal processes in the production and their influences on performance of asphalt mixtures with reclaimed asphalt pavement (RAP). *Constr. Build. Mater.* **2019**, *206*, 609–619. [CrossRef]
9. Wang, Z.; Liu, D.; Hu, B.; Zhu, C.; Luo, W. An improved regression model to predict fatigue life of asphalt mixes incorporating low to moderate RAP contents. *Constr. Build. Mater.* **2023**, *374*, 130904. [CrossRef]
10. Yang, C.; Zhang, J.; Yang, F.; Cheng, M.; Wang, Y.; Amirkhanian, S.; Wu, S.; Wei, M.; Xie, J. Multi-scale performance evaluation and correlation analysis of blended asphalt and recycled asphalt mixtures incorporating high RAP content. *J. Clean. Prod.* **2021**, *317*, 128278. [CrossRef]
11. Qiao, Y.; Wen, X.; Liu, S.; Lv, S.; He, L. Stochastic analysis for comparing life cycle carbon emissions of hot and cold mix asphalt pavement systems. *Resour. Conserv. Recycl.* **2025**, *212*, 107881. [CrossRef]
12. Li, N.; Cheng, Z.; Tang, W.; Fan, X.; Yi, Z. Uniformity and mechanical performance of recycled asphalt mixtures with high RAP content based on refined decomposition: A comparative study with conventional separation. *Mater. Struct.* **2025**, *58*, 276. [CrossRef]
13. Bharathi, V.P.N.; Muthuswamy, K.; Balakrishnan, B.N.; Jothiprakash, G.; Shanmugam, K.; Loganathan, K.; Vasudevan, B.; Appavu, S.; Marimuthu, R.; Rajaram, D.; et al. A comparative analysis and prediction of carbon emission in India using machine learning models. *Glob. NEST J.* **2025**, *27*, 06020. [CrossRef]
14. Zhu, D.; Ma, R.; Liu, J.; Li, X.; Sha, J. A new method for predicting carbon emissions in energy industry based on CEEMD wavelet denoising and hybrid machine learning. *Energy Rep.* **2025**, *14*, 3132–3141. [CrossRef]
15. Mujeeb, S.; Javaid, N. Deep learning based carbon emissions forecasting and renewable energy's impact quantification. *IET Renew. Power Gener.* **2023**, *17*, 873–884. [CrossRef]
16. Wang, C.; Li, M.; Yan, J. Forecasting carbon dioxide emissions: Application of a novel two-stage procedure based on machine learning models. *J. Water Clim. Change* **2023**, *14*, 477–493. [CrossRef]
17. Yang, W.; Chen, L.; Ke, T.; He, H.; Li, D.; Liu, K.; Li, H. Carbon Emission Trend Prediction for Regional Cities in Jiangsu Province Based on the Random Forest Model. *Sustainability* **2024**, *16*, 10450. [CrossRef]
18. Zhao, Y.; Liu, R.; Liu, Z.; Liu, L.; Wang, J.; Liu, W. A Review of Macroscopic Carbon Emission Prediction Model Based on Machine Learning. *Sustainability* **2023**, *15*, 6876. [CrossRef]
19. Zhang, X.; Sun, J.; Zhang, X.; Wang, F. Assessment and regression of carbon emissions from the building and construction sector in China: A provincial study using machine learning. *J. Clean. Prod.* **2024**, *450*, 141903. [CrossRef]
20. Ji, Y.; Wen, S.; Zhao, Y.; Niu, D.; Ding, Z. A review of life cycle assessment of carbon emissions from recycled asphalt pavement. *J. South China Univ. Technol. (Nat. Sci. Ed.)* **2026**, *54*, 179–190.
21. Naser, M.Z. Causality and causal inference for engineers: Beyond correlation, regression, prediction and artificial intelligence. *WIREs Data Min. Knowl. Discov.* **2024**, *14*, e1533. [CrossRef]
22. Naser, M.Z. Discovering causal models for structural, construction and defense-related engineering phenomena. *Def. Technol.* **2025**, *43*, 60–79. [CrossRef]
23. Tan, X.; Xing, J.; Mahjoubi, S.; Guo, P.; Wei, Z.; Wang, Y.; Ren, J.; Ai, L.; Meng, W.; Bao, Y. Explainable machine learning and life cycle assessment for sustainable design of fiber-reinforced asphalt concrete. *J. Clean. Prod.* **2026**, *547*, 147759. [CrossRef]
24. *DB15/T 3727-2024[S]*; Technical Specification for Carbon Emission Accounting of Ultra-Thin Wearing Course Using Warm-Mix Recycled Asphalt Mixture. Market Supervision Administration of Inner Mongolia Autonomous Region: Hohhot, China, 2024.
25. *JTG B01-2014[S]*; Technical Standard of Highway Engineering. China Communications Press: Beijing, China, 2014.

26. Wang, M.; Wang, C.; Gao, X.; Gao, F.; Xiao, X. A review of cold recycling technology of emulsified asphalt for highway pavement. *Mater. Rep.* **2023**, *37*, 50–60.
27. Luo, P.; Li, P.; Yang, W.; Li, W. Evaluation of asphalt aging degree based on grey correlation and factor analysis. *Chem. Ind. Eng. Prog.* **2025**, *44*, 5108–5119. [CrossRef]
28. Li, H.; Xiong, X.; Li, J. Experimental analysis on performance of SMA recycled asphalt mixture with different RAP contents. *J. China Foreign Highw.* **2022**, *42*, 242–246. [CrossRef]
29. Fu, H.; Guo, K. Study on pavement performance of warm recycled asphalt mixture. *West. China Commun. Sci. Technol.* **2021**, *167*, 32–38. [CrossRef]
30. *JTG/T 3832-2018[S]*; Budget Quota of Highway Engineering. China Communications Press: Beijing, China, 2018.
31. China Carbon Emission Trading Market. *National Carbon Market Trading Price Report*; Shanghai Environment and Energy Exchange: Shanghai, China, 2023.
32. China Materials Engineering Canon Editorial Committee. *China Materials Engineering Canon*; Chemical Industry Press: Beijing, China, 2006.
33. Yang, S.; Tao, W. *Heat Transfer*, 4th ed.; Higher Education Press: Beijing, China, 2006.
34. Schönauer, P.; Gruber, M.R.; Hofko, B. Case study of a batch asphalt mix plant: Energy consumption and emission allocation based on primary data. *Case Stud. Constr. Mater.* **2024**, *21*, e03669. [CrossRef]
35. Wang, C.; Zhang, Y.; Fang, X.; Hu, T.; Suo, Z.; Gong, C.; Li, J. Construction of energy consumption model in asphalt mixture production stage based on field measurements. *Buildings* **2024**, *14*, 3303. [CrossRef]
36. Schönauer, P.; Gruber, M.R.; Hofko, B. Impact of aggregate moisture on dryer drum energy demand in asphalt mixture production: Field trial and model validation. *Constr. Build. Mater.* **2026**, *521*, 146151. [CrossRef]
37. Kleizienė, R.; Buttitta, G.; Carreño, N.; Lo Presti, D. Enhancing the sustainability of asphalt mixtures: A focus on operational factors and dataset for environmental product declarations. *Sustainability* **2025**, *17*, 9349. [CrossRef]
38. Liu, Y.; Yang, J.; Wang, H.; Liu, S.; Fan, Y.; Zhou, Y.; Gong, M.; Huang, W. Energy consumption and carbon emissions of mixing plant in asphalt pavement construction with a case study in China and reduction measures. *Case Stud. Constr. Mater.* **2025**, *22*, e04165. [CrossRef]
39. Natural Resources Canada. *Energy Benchmarking and Best Practices in Canadian Road Building /Heavy Construction Sector*; Government of Canada: Ottawa, ON, Canada, 2005.
40. Ma, F.; Sha, A.; Lin, R.; Huang, Y.; Wang, C. Greenhouse gas emissions from asphalt pavement construction: A case study in China. *Int. J. Environ. Res. Public Health* **2016**, *13*, 351. [CrossRef] [PubMed]
41. Chen, T.; Guestrin, C. XGBoost: A scalable tree boosting system. In Proceedings of the 22nd ACM SIGKDD International Conference on Knowledge Discovery and Data Mining, New York, NY, USA, 13–17 August 2016; pp. 785–794. [CrossRef]

Disclaimer/Publisher's Note: The statements, opinions and data contained in all publications are solely those of the individual author(s) and contributor(s) and not of MDPI and/or the editor(s). MDPI and/or the editor(s) disclaim responsibility for any injury to people or property resulting from any ideas, methods, instructions or products referred to in the content.